MFN= 008666
01 SID/SCD
02 7316
03 INPE-7316-PRE/3211
04 CEA
05 S
06 as
10 Tsurutani, Bruce T.
10 Gonzalez-Alarcon, Walter Demetrio
10 Gonzalez-Alarcon, Alicia Luisa Clua
10 Tang, Frances
10 Arballo, John K.
10 okada, Masaki
12 Interplanetary origin of geomagnetic activity in the declining phase of the solar cycle
14 21717-21733
30 Journal of geophysical Research
31 100
32 A11
40 En
41 En
58 DGE
61 <PI>
64 Nov. <1995>
68 PRE
76 GEOFISICA ESPACIAL
83 Interplanetary magnetic field (IMF) and plasma data are compared with ground-based geomagnetic Dst and AE indices to determine the causes of magnetic storms, substorms, and quiet during the descending phase of the solar cycle. In this paper we focus primarily on 1974 when the AE index is anomalously high (AE = 283 nT). This year is characterized by the presence of two long-lasting corotating streams associated with coronal holes. The corotating streams interact with the upstream low-velocity (300-350 km s-1), high-density heliospheric current sheet (HCS) plasma sheet, which leads to field compression and ~15 to 25-nT hourly average values. Although the Bz component in this corotating interaction region (CIR) is often < -10 nT, typically the field directionality is highly variable, and large southward components have durations less than 3 hours. Thus the corotating strean/HCS plasma sheet interaction region can cause recurring moderate (-100 nT:5 Dst... -50 nT) to weak (50 nT...Dst:5 -25 nT) storms, and sometimes no significant ring current activity at all (Dst > -25 nT). Storms of major (Dst... - 100 nT) intensities were not associated with CIRs. Solar wind energy is transferred to the magnetosphere via magnetic reconnection during the weak and moderate storms. Because the B, component in the interaction region is typically highly fluctuating, the corresponding storm main phase profile is highly irregular. Reverse shocks are sometimes present at the sunward edge of the CIR. Because these events cause sharp decreases in field magnitude, they can be responsible for storm

recovery phase onsets. The initial phases of these corotating stream-related storms are caused by the increased ram pressure associated with the HCS plasma sheet and the further density enhancement from the stream-stream compression. Although the solar wind speed is generally low in this region of space, the densities can be well over an order of magnitude higher than the average value, leading to significant positive Dst values. Since there are typically no forward shocks at 1 AU associated with the stream-stream interactions, the initial phases have gradual onsets. The most dramatic geomagnetic response to the corotating streams are chains of consecutive substorms caused by the southward components of large-amplitude Alfven waves within the body of the corotating streams. This auroral activity has been previously named high-intensity long-duration continuous AE activity (HILDCAAs). The substorm activity is generally most intense near the peak speed of the stream where the Alfven wave amplitudes are greatest, and it decreases with decreasing wave amplitudes and stream speed. Each of the 27-day recurring HILDCAA events can last 10 days or more, and the presence of two events per solar rotation is the cause of the exceptionally high AE average for 1974 (higher than 1979). HILDCAAs often occur during the recovery phase of magnetic storms, and the fresh (and sporadic) injection of substorin energy leads to unusually long storm recovery phases as noted in Dst In the far trailing edge of the corotating stream, the IMF amplitudes become low, <3 nT, and there is an absence of large-amplitude fluctuations (Alfven waves). This is related to and causes geomagnetic quiet. There were three major (Dst... -100 nT) storms that occurred in 1974. Each was caused by a nonrecurring moderate speed stream led by a fast forward shock. The mechanisms for generating the intense interplanetary B, which were responsible for the subsequent intense magnetic storms was shock compression of preexisting southwardly directed Bz (Bs) for the two largest events and a magnetic cloud for the third (weakest) event. Each of the three streams occurred near a HCS crossing with no obvious solar optical or X ray signatures. It is speculated that these events may be associated with flux openings associated with coronal hole expansions. In conclusion, we present a model of geomagnetic activity during the descending phase of the solar cycle. It incorporates storm initial phases, main phases, HILDCAAs, and geomagnetic quiet. It uses some of the recent Ulysses results. We feel that this model is sufficiently developed that it may be used for predictions, and we encourage testing during the current Dhase of the solar cycle.

87 MAGNETOSFERA
87 TEMPESTADES MAGNETICAS
87 CICLO SOLAR
90 b
91 FDB-20000106
92 FDB-MLR

responsible for storm recovery phase onsets. The initial phases of these corotating stream-related storms are caused by the increased ram pressure associated with the HCS plasma sheet and the further density enhancement from the stream-stream compression. Although the solar wind speed is generally low in this region of space, the densities can be well over an order of magnitude higher than the average value, leading to significant positive Dst values. Since there are typically no forward shocks at 1 AU associated with the stream-stream interactions, the initial phases have gradual onsets. The most dramatic geomagnetic response to the corotating streams are chains of consecutive substorms caused by the southward components of large-amplitude Alfvén waves within the body of the corotating streams. This auroral activity has been previously named high-intensity long-duration continuous AE activity (HILDCAAs). The substorm activity is generally most intense near the peak speed of the stream where the Alfvén wave amplitudes are greatest, and it decreases with decreasing wave amplitudes and stream speed. Each of the 27-day recurring HILDCAA events can last 10 days or more, and the presence of two events per solar rotation is the cause of the exceptionally high AE average for 1974 (higher than 1979). HILDCAAs often occur during the recovery phase of magnetic storms, and the fresh (and sporadic) injection of substorin energy leads to unusually long storm recovery phases as noted in D$_{st}$. In the far trailing edge of the corotating stream, the IMF amplitudes become low, <3 nT, and there is an absence of large-amplitude fluctuations (Alfvén waves). This is related to and causes geomagnetic quiet. There were three major (Dst $\leq$ -100 nT) storms that occurred in 1974. Each was caused by a nonrecurring moderate speed stream led by a fast forward shock. The mechanisms for generating the intense interplanetary B, which were responsible for the subsequent intense magnetic storms was shock compression of preexisting southwardly directed B_z (B_s) for the two largest events and a magnetic cloud for the third (weakest) event. Each of the three streams occurred near a HCS crossing with no obvious solar optical or X ray signatures. It is speculated that these events may be associated with flux openings associated with coronal hole expansions. In conclusion, we present a model of geomagnetic activity during the descending phase of the solar cycle. It incorporates storm initial phases, main phases, HILDCAAs, and geomagnetic quiet. It uses some of the recent Ulysses results. We feel that this model is sufficiently developed that it may be used for predictions, and we encourage testing during the current Dhase of the solar cycle.

87 MAGNETOSFERA
87 TEMPESTADES MAGNETICAS
87 CICLO SOLAR
90 b
91 FDB-20000106
92 FDB-MLR

JOURNAL OF GEOPHYSICAL RESEARCH, VOL. 100, NO. A11, PAGES 21,717–21,733, NOVEMBER 1, 1995

Interplanetary origin of geomagnetic activity in the declining phase of the solar cycle

Bruce T. Tsurutani,[1] Walter D. Gonzalez,[2] Alicia L. C. Gonzalez,[2] Frances Tang,[3] John K. Arballo,[1] and Masaki Okada[4]

Abstract. Interplanetary magnetic field (IMF) and plasma data are compared with ground-based geomagnetic *Dst* and *AE* indices to determine the causes of magnetic storms, substorms, and quiet during the descending phase of the solar cycle. In this paper we focus primarily on 1974 when the *AE* index is anomalously high ($\overline{AE}$ = 283 nT). This year is characterized by the presence of two long-lasting corotating streams associated with coronal holes. The corotating streams interact with the upstream low-velocity (300-350 km s^{-1}), high-density heliospheric current sheet (HCS) plasma sheet, which leads to field compression and ~15- to 25-nT hourly average values. Although the B_z component in this corotating interaction region (CIR) is often < -10 nT, typically the field directionality is highly variable, and large southward components have durations less than 3 hours. Thus the corotating stream/HCS plasma sheet interaction region can cause recurring moderate (-100 nT ≤ *Dst* ≤ -50 nT) to weak (-50 nT ≤ *Dst* ≤ -25 nT) storms, and sometimes no significant ring current activity at all (*Dst* > -25 nT). Storms of major (*Dst* ≤ -100 nT) intensities were not associated with CIRs. Solar wind energy is transferred to the magnetosphere via magnetic reconnection during the weak and moderate storms. Because the B_z component in the interaction region is typically highly fluctuating, the corresponding storm main phase profile is highly irregular. Reverse shocks are sometimes present at the sunward edge of the CIR. Because these events cause sharp decreases in field magnitude, they can be responsible for storm recovery phase onsets. The initial phases of these corotating stream-related storms are caused by the increased ram pressure associated with the HCS plasma sheet and the further density enhancement from the stream-stream compression. Although the solar wind speed is generally low in this region of space, the densities can be well over an order of magnitude higher than the average value, leading to significant positive *Dst* values. Since there are typically no forward shocks at 1 AU associated with the stream-stream interactions, the initial phases have gradual onsets. The most dramatic geomagnetic response to the corotating streams are chains of consecutive substorms caused by the southward components of large-amplitude Alfvén waves within the body of the corotating streams. This auroral activity has been previously named high-intensity long-duration continuous *AE* activity (HILDCAAs). The substorm activity is generally most intense near the peak speed of the stream where the Alfvén wave amplitudes are greatest, and it decreases with decreasing wave amplitudes and stream speed. Each of the 27-day recurring HILDCAA events can last 10 days or more, and the presence of two events per solar rotation is the cause of the exceptionally high *AE* average for 1974 (higher than 1979). HILDCAAs often occur during the recovery phase of magnetic storms, and the fresh (and sporadic) injection of substorm energy leads to unusually long storm recovery phases as noted in *Dst*. In the far trailing edge of the corotating stream, the IMF amplitudes become low, <3 nT, and there is an absence of large-amplitude fluctuations (Alfvén waves). This is related to and causes geomagnetic quiet. There were three major (*Dst* ≤ -100 nT) storms that occurred in 1974. Each was caused by a nonrecurring moderate speed stream led by a fast forward shock. The mechanisms for generating the intense interplanetary B_s which were responsible for the subsequent intense magnetic storms was shock compression of preexisting southwardly directed B_z (B_s) for the two largest events and a magnetic cloud for the third (weakest) event. Each of the three streams occurred near a HCS crossing with no obvious solar optical or X ray signatures. It is speculated that these events may be associated with flux openings associated with coronal hole expansions. In conclusion, we present a model of geomagnetic activity during the descending phase of the solar cycle. It incorporates storm initial phases, main phases, HILDCAAs, and geomagnetic quiet. It uses some of the recent Ulysses results. We feel that this model is sufficiently developed that it may be used for predictions, and we encourage testing during the current phase of the solar cycle.

Paper number 95JA01476.
0148-0227/95/95JA-01476$05.00

[1]Jet Propulsion Laboratory, California Institute of Technology, Pasadena.
[2]Instituto National Pesquisas Espaciais, Sao Jose dos Campos, Sao Paulo, Brazil.
[3]California Institute of Technology, Pasadena.
[4]National Institute of Polar Research, Tokyo, Japan.

Introduction

Recently, considerable attention has focused on the interplanetary and solar causes of geomagnetic storms (here we use the *Gonzalez et al.* [1994] definition of a magnetic storm as an event with substantially negative *Dst*) that have occurred at and near solar maximum [*Gonzalez and Tsurutani*, 1987; *Burlaga et al.*, 1987; *Tsurutani et al.*, 1988, 1992; *Tang et al.*, 1989; *Gonzalez et al.*, 1989, 1992, 1994; *Gosling et al.*, 1990, 1991; *Hoeksema and Zhao*, 1992; *Crooker et al.*, 1992a; *Farrugia* et *al.*, 1993a, b; *Tsurutani and Gonzalez*, 1995a]. Almost all of the large storm events were associated with fast ejecta that have impinged upon the Earth's magnetosphere. The mechanisms causing the geomagnetic activity have been shown to be compressed southward directed magnetic fields (B_s) behind interplanetary shocks [*Tsurutani et al.*, 1988] or southward fields within the magnetic cloud [*Burlaga, et al.*, 1981; *Klein and Burlaga*, 1982] portion of the driver gases (see *Gonzalez et al.* [1994] for a review). Magnetic reconnection [*Dungey, 1961*] between the interplanetary and magnetopause fields is the energy transfer mechanism creating the storms.

During the descending phase of the solar cycle, high-velocity solar ejecta occur less frequently, and corotating high-speed streams occur more often [*Feynman and Gu*, 1986]. The corotating streams have been associated with polar coronal holes [*Krieger et al.*, 1973, 1974; *Timothy et al.*, 1975] that have extended to latitudes close to the ecliptic plane [*Burlaga et al.*, 1978]. Because the holes are (relatively) fixed at the Sun, the high-speed streams "corotate" with the Sun's ~27 day rotation rate [*Timothy* et *al.*, 1975].

It has been known for a long time [*Bartels*, 1938; *Chapman and Bartels*, 1940; *Dessler and Fejer*, 1963] that moderate level geomagnetic activity can occur with a ~27 day period. Clearly, it is the corotating streams [*Burlaga and Lepping*, 1977; *Sheeley et al.*, 1977; *Burlaga et al.*, 1978], the preceding heliospheric current sheet (HCS) crossings [*Smith et al.*, 1978], or the stream-stream interaction regions [*Belcher and Davis*, 1971; *Pizzo*, 1985] that are responsible for such geomagnetic activity. It is the purpose of this paper to determine what solar wind plasma and magnetic field features are responsible for geomagnetic storms, substorms, and geomagnetic quiet during the descending phase of the solar cycle when the corotating streams dominate in occurrence rate over fast ejecta. There are several reasons to expect that the cause of geomagnetic activity will be considerably different than during solar maximum. The corotating streams are not expected to have embedded magnetic clouds with intense southward fields. Also, because the plasma is continuously emitted from the coronal holes, fast forward (and reverse) shocks should only form at the corotating interaction region (CIR) boundaries [*Smith and Wolfe*, 1976]; for example, see Figure 13 of *Belcher and Davis* [1971]. Pioneer 10 and 11 observations have shown that fast forward shocks associated with corotating streams typically do not form until ~1.5 AU from the Sun, and reverse shocks not until ~2.5 AU [*Smith and Wolfe*, 1976]. The absence of a forward shock at the antisolar edge of a fast stream and a ~27-day recurrence of the stream has been used to identify such corotating structures.

This paper will attempt to build on previous solar wind works which have dealt with the plasma density enhancements near heliosphere current sheets [*Belcher and Davis*, 1971; *Burlaga et al*, 1978; *Borrini et al.*, 1981], high-speed corotating streams adjacent to the HCS plasma sheet [*Sheeley et al.*, 1976, 1977; *Gosling et al.*, 1976] (these structures have been called HCS plasma sheets by *Winterhalter et al.* [1994]), magnetic sector

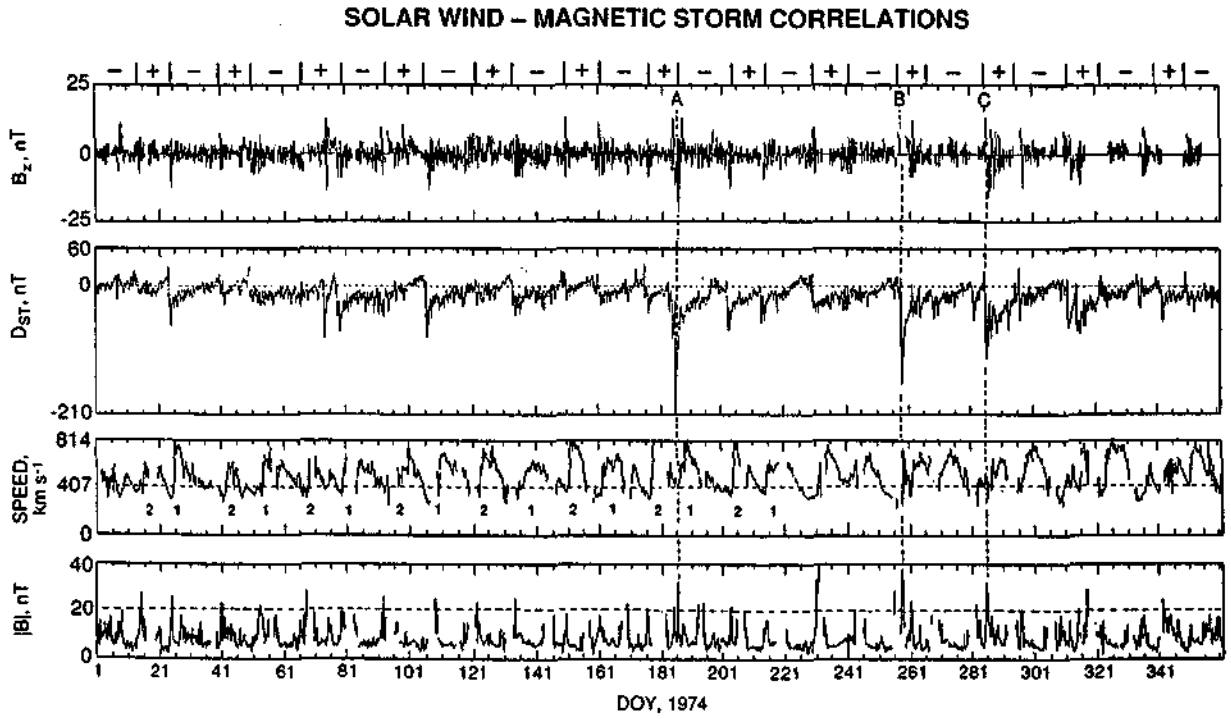

Figure 1. The IMF B_Z, *Dst*, V_{SW}, and IMF |*B*| for 1974. Two sequences of corotating streams are indicated in the solar wind speed panel. These streams are responsible for moderate to weak magnetic storms. The three largest intensity magnetic storms are called out as the A, B, and C events. These storms are caused by fast ejecta from the Sun and are not related to corotating streams. The sectors are denoted at the top of the figure.

structures or heliospheric current sheets [*Ness and Wilcox*, 1964; *Wilcox and Ness* 1965; *Smith et al.*, 1978], high-speed corotating streams adjacent to the HCS plasma sheet [*Sheeley et al.*, 1976, 1977; *Gosling et al.*, 1976], and stream-stream magnetic field compressive effects [*Burlaga et al.*, 1977, 1978]. The purpose of this paper will be to put the above structures into context and to specifically address the nature of the interplanetary magnetic field (IMF) B_z component, which will be shown to be the primary factor in causing geomagnetic activity/lack of activity during the descending phase of the solar cycle.

Data Selection and Method of Analyses

We have selected three years during the descending phase of solar cycle 20 for this study (1973-1975). This particular interval was chosen because of the presence of two long-lasting coronal holes that provided corotating high-speed streams in the interplanetary medium [*Hansen et al.*, 1976; *Burlaga et al.*, 1978; *Tsurutani et al.*, 1982; *Lindblad and Lundstedt*, 1983; *Lindblad*, 1990]. Although all three years have been analyzed, for purposes of illustration we will focus primarily on the data from 1974. This year contains the cleanest, most unambiguous examples of recurring streams and is representative of the three years of study.

In order to perform this study, both low temporal resolution (~1 hour) and high-resolution (seconds to minutes) magnetic field and plasma data are used. The former will be used to illustrate the large-scale timing features of the high-speed streams and HCS plasma sheet events, and the latter to study the detailed causes of the southward B_z (B_S) events. We have used the OMNI 1-hour averages of the interplanetary parameters for the former and have also obtained high-resolution IMP 7 and 8 plasma and magnetic field data from the National Space Science Data Center, Goddard Space Flight Center, for the latter. Because the IMP spacecraft are Earth-orbiting, there are interplanetary data gaps when the satellites enter the magnetosphere/magnetotail. These gaps unfortunately cannot be avoided. For the high-resolution data, the gaps are filled with straight lines. *Dst* (1 hour) and *AE* (2.5 min) indices are used to indicate geomagnetic storm activity and substorm activity, respectively. The 2.5-min *AE* indices were averaged to 1 hour where appropriate. *Dst* has been shown to be linearly related to the total ring current particle energy by *Sckopke* [1966], and we use this index as a proxy for the latter. Three-hour *ap* indices are shown as well. These indices were obtained from the World Data Center A (WDC-A), Boulder, Colorado.

We use the WDC-A uncorrected *Dst* indices throughout the paper. Intervals such as the initial phases of storms can be better studied without introducing pressure corrections; thus our usage of raw values. It should be noted, however, that for some main phase intervals, the uncorrected values can depart from the corrected values. Thus some storm intensities might be greater than those shown in this paper.

Results

High-Speed Corotating Streams and Associated Magnetic Field Structures

Figures 1 and 2 illustrate hourly averages of the magnetic field and plasma data and geomagnetic indices for the year 1974. These figures are shown to give an overview of the geomagnetic activity for the entire year (high-resolution plots are available upon request from the authors). In Figure 1, from top to bottom, are the interplanetary magnetic field B_z component in GSM coordinates, *Dst*, the solar wind speed, and the magnetic field magnitude. In the GSM coordinate system, $\hat{x}$ is toward the Sun, $\hat{y}$ is defined by $\hat{n} \times \hat{x}/|\hat{n} \times \hat{x}|$, and $\hat{z}$ forms a right-hand system. Here $\hat{n}$ is the south magnetic pole direction. Figure 2, to the same scale, has GSM B_x, B_y, solar wind proton density, and

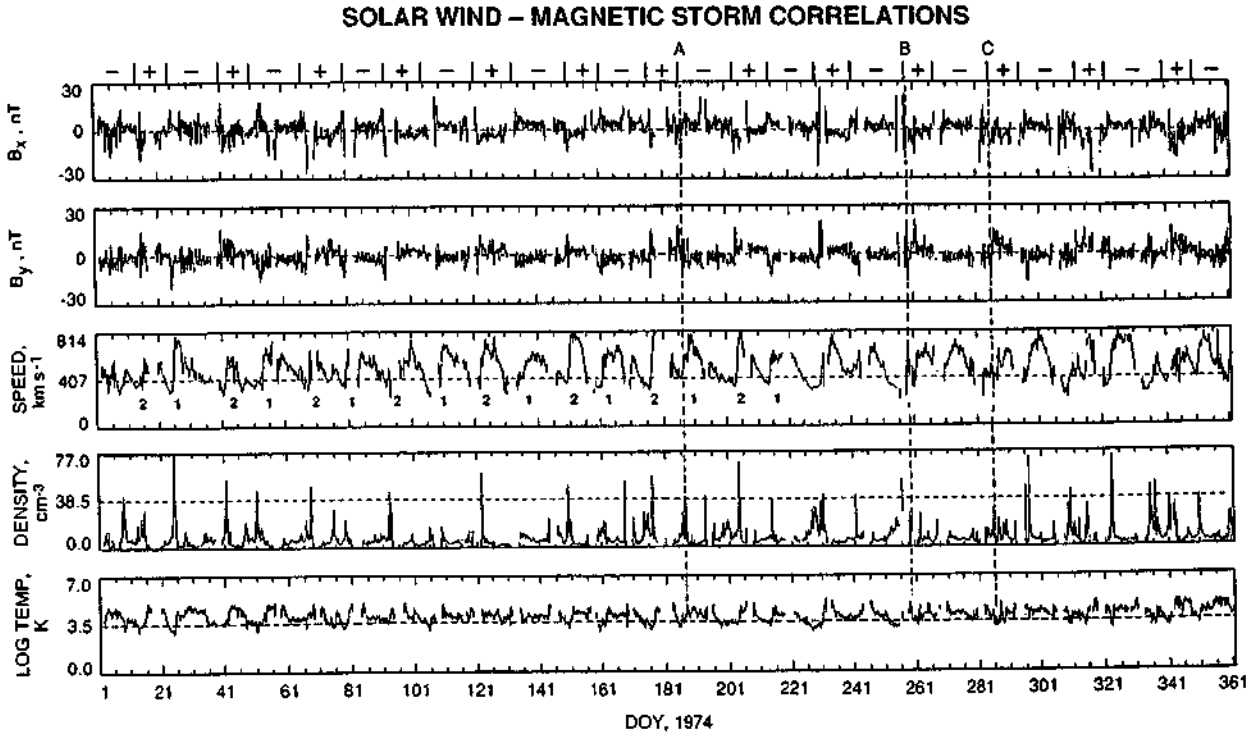

Figure 2. Same format as Figure 1, but for IMF B_x, B_y, V_{SW}, N and T.

temperature. Solar wind speed is repeated in the middle panel of Figure 2 as a reference, so that this figure can be related to features in Figure 1. At the top of both figures, the IMF sectors are indicated, with the plus and minus signs indicating positive and negative sectors. Positive sectors are those in which the fields are directed outward from the Sun.

There are several important points to note in Figure 1. The first is that there are many high-speed streams present (sometimes more than two per solar rotation) with peak speeds up to 800 km s^{-1}. Most streams have a characteristic profile of a fast rise in speed and a long decay [*Neugebauer and Snyder*, 1966]. Some excellent examples of this are the three streams within days 24-68 and the three streams within days 177-214. Other streams have profiles which indicate that the streams are composed of several partially overlapping events. Examples of the latter can be found within days 161-176 (with "small-amplitude" stream onsets on days 162, 163, 166, and 171) and within days 25-41 (with onsets on days 25, 28, and 30).

In Figure 1, two main recurring streams are present in the first two thirds of the year. Stream onsets are present for the consecutive 27-day periods of days 24, 51, 78, 105, 132, 159, 186, 213, and 240. This sequence also extends back in time into 1973 and also forward into 1975, but with less regularity than the events discussed above. We will refer to this recurring stream as the sequence 1 stream. A second sequence of streams is located between the sequence 1 streams, with onsets on days 15, 41, 68, 95, 122, 150, 177, 204, and 231. This second recurring stream will be called the sequence 2 stream. None of these streams had fast forward shocks, in agreement with the *Smith and Wolf* [1976] empirical model. Beyond day 231 the streams become somewhat more complex, so we will focus on the first two thirds of the year.

The bottom panel of Figure 1 shows the hourly averages of the magnetic field magnitude. The highest field magnitudes that occurred during the year are located near the leading edges of the high-speed streams. Almost all of the large fields that have hourly averages greater than 15 nT are of this type. Examples are present on days 25-26, 150-151, 161-162, 176-177, 187, and 204. The maximum (hourly average) intensities for these events lie in the range of 10 to 25 nT.

There were only four cases where hourly average field strengths exceeded 30 nT. These events occurred on days 187, 232, 258, and 286. Three of these events are associated with major ($Dst \leq$ -100 nT) magnetic storms, labeled the A, B, and C events. Each is associated with a solar ejecta event and not with a corotating stream. This will be discussed in depth later.

Interplanetary Events Causing Magnetic Storms (*Dst*)

The second panel of Figure 1 is the hourly average *Dst* values for the year. There are two notable features in this panel. The first is that there are only a few major ($Dst \leq$ -100 nT) magnetic storms during the entire year. These are the previously mentioned event A, on day 187 (Dst = -205 nT), event B on day 257 (Dst = -140 nT), and event C on day 285 (Dst = -115 nT). All three of the high-speed stream events are led by fast forward shocks (shown later). These streams do not recur at 27-day intervals (it is noted however, that the latter two events are separated by 28 days).

The next highest level of magnetic storm intensities during 1974 occurs in a narrow range of -85 nT $\leq Dst \leq$ -70 nT. There are four storms in this grouping, and they occur on days 75, 80, 108, and 204. Each of the events is associated with large, ~15-nT (hourly average) interplanetary magnetic field magnitudes. These large fields are located in and near the high-velocity/low-velocity stream interfaces. The stream events on days 80 and 108 are sequence 1 corotating streams. The stream event on day 204 is a sequence 2 stream. The event on day 75 is a smaller, impulsive stream located between the two main sequence corotating streams.

The storm intensities associated with the nicely periodic (27-day) sequence 1 and 2 stream structures are only modest at best. As noted above, from day 1 to day 241, during nine solar rotations and 18 major corotating stream appearances, there were only three stream appearances associated with $Dst \leq$ -70 nT values. Most (12 of 18 events) of the above high-speed streams cause only small Dst disturbances of $Dst \geq$ -50 nT. Sometimes the geomagnetic disturbances were not even perceptible in Dst. Examples of this latter type of small ($\geq$ -25 nT) disturbance, or no storm at all are present on days 15, 41, 68, 95, 123, 134, 150, 162, 177, 231, and 241. The peak speed gradient and peak magnetic fields of these streams are not much different from those that cause storms with intensities of $Dst \leq$ -70 nT, however.

The top panel of Figure 1 is the IMF B_z component in GSM coordinates. Large, southward B_z spikes are coincident with storms with -85 nT $\leq Dst \leq$ -70 nT. Examples can be found on days 74-75, 80, 108, and 204. Other large southward B_z spikes (< -10 nT) can be noted on days 24-25, 75 and 214. These events are related to moderate intensity storms. Presumably, magnetic reconnection is the mechanism of solar wind energy input into the magnetosphere for these events.

Geoeffectiveness of the Two Corotating Steam Sequences

The two streams, sequences 1 and 2, vary in their geoeffectiveness from solar rotation to rotation and over their stream lifetimes. Of the two sequences, the first is more geoeffective at the beginning of the interval studied. Sequence 1, starting on day 25 and progressing at 27-day intervals, caused peak Dst values of -65, -20, -75, -85, -45, -30, "A," -60, and -35 nT. The seventh event of the sequence near event A is indeterminate because the large "A" storm overshadows any activity associated with the corotating stream. From Figure 1 the reader can note that the speed of the stream decreases steadily throughout the sequence. The peak speed starts near ~ 800 km s^{-1} and declines to ~ 600 km s^{-1} near the end of the sequence.

Sequence 2, starting at day 15 (and progressing at 27-day intervals) caused peak Dst values of -20, -20, -30, -50, -30, -25, -40, -75, and -35 nT. The peak speeds of the streams at the beginning of the sequence have values of ~600-650 km s^{-1}. This value rises more or less continuously throughout the sequence until a peak speed of 800-850 km s^{-1} is reached for the last four appearances of the stream. A sharp magnetic spike of magnitude 15-20 nT is present at the high-speed stream-slow stream interaction regions during the last appearances of this sequence. Again, there is not a direct relationship between peak solar wind speed and Dst.

It should be noted that previous studies have described the general relationship between solar wind speed and geomagnetic activity during this phase of the solar cycle. *Sheeley et al.* [1976, 1977] and *Gosling et al.* [1976] have examined the same interval of time (and other intervals as well) and have come up with similar but more general conclusions.

Positive *Dst* Intervals

Two other features in the Dst plot are noteworthy. One is that there are several intervals where Dst has positive (~ +10 to +20 nT) values for several days at a time. These features can be

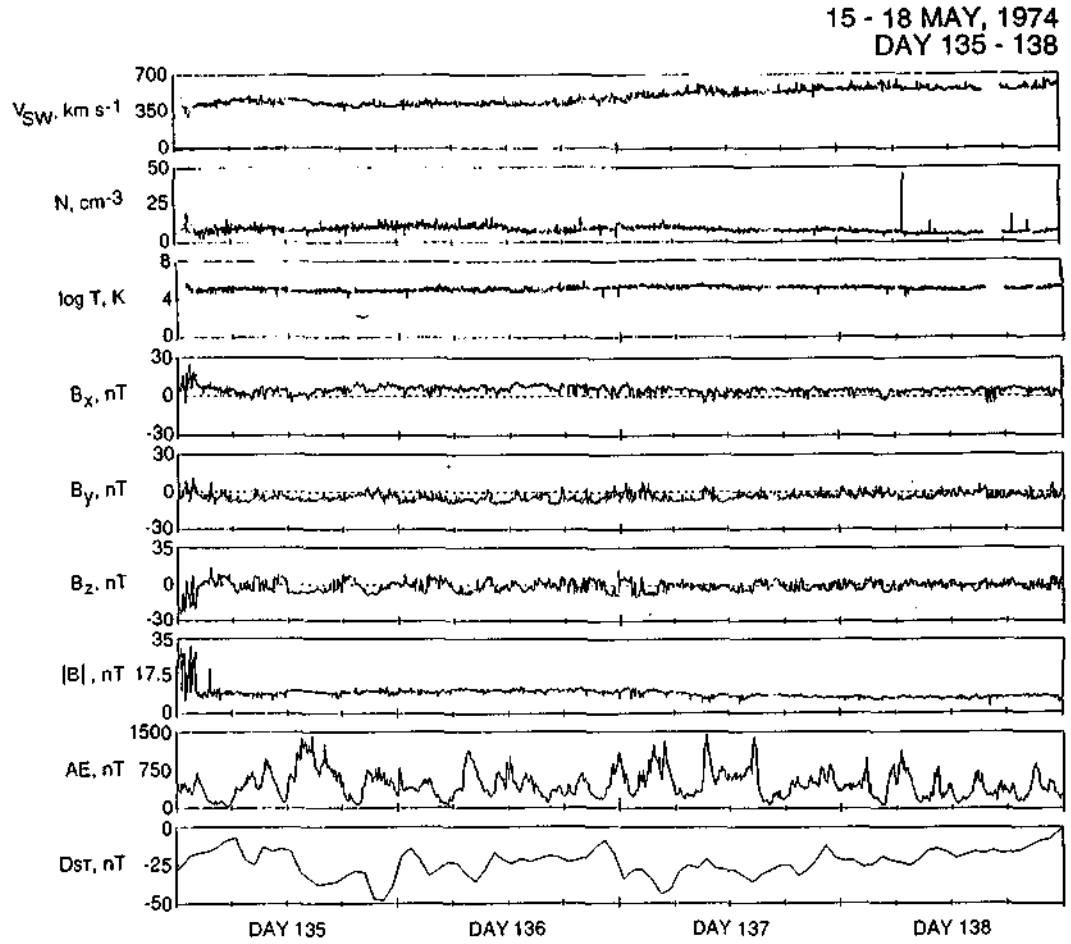

Figure 3. *Dst* in a "recovery" phase of a magnetic storm. V_{SW}, N, T, the IMF, AE and *Dst* or days 135 through 138, 1974. The ring current does not have a classic decay profile, but *Dst* stays within the range of ~ -10 to -50 nT for days. Short *Dst* decreases are accompanied by southward B_z (B_S) events and AE increases. Presumably, magnetic reconnection through the B_z southward turnings causes the injection of fresh plasma into the magnetosphere, leading to small enhancements of the ring current.

related to specific solar wind parameters. Examples of positive *Dst* events are found on days 14, 40, 50, 78, 105, 132, and 227. The onsets of these events are gradual, and the magnitude of *Dst* typically increases with time. The events start days before the appearance of the high-speed streams. Each event is associated with a slow solar wind stream located between the two high-speed coronal hole streams. For the events mentioned above, the minimum solar wind speed was approximately 350, 310, 330, 330, 310, 330, and 300 km s^{-1}, respectively. The densities during these intervals are 20, 10, 7, 12, 10, 8, and 30 cm^{-3}, which are either typical of solar wind densities or slightly on the high side. These values increase with time to 20, 44, 38, 20, 30, 12, and 40 cm^{-3}. Although the solar wind speeds are low, the high plasma densities cause an increased ram pressure and thus the positive *Dst* values.

Dst Recovery

Another feature to note in the *Dst* panel of Figure 1 is the very long recovery phases for the small magnetic storms generated by the corotating high-speed streams. Most recoveries last 1 week or longer, sometimes even until the next stream arrives. This is substantially different from what happens with storms that occur at and near solar maximum (a standard decay time of the solar maximum storms is <10 hours [*Gonzalez et al.*, 1989]. In this epoch, long recovery phases are the rule rather than the exception. Some prime examples of this are found on days 25 to 35, 80 to 92, and 108 to 122 for the sequence 1 streams and days 204 to 214 and 231 to 241 for the sequence 2 streams. Many other examples are present in the figure and for those in 1973 and 1975 (not shown).

Some storm "recoveries" have *Dst* negative intensities which are relatively constant for days on end. Two good examples of this feature are present on days 52-60 and 135-138. Both of these events are associated with sequence 1 streams. On day 52 the *Dst* event onset coincides with a very small amplitude precursor solar wind stream prior to the main, high-speed stream, and the *Dst* depression continues well into and beyond the speed peak.

The days 135-138 event is shown in higher temporal resolution in Figure 3. The panels are the solar wind plasma parameters, plus interplanetary magnetic field components and magnitude, and AE and *Dst*. There is a moderate speed precursor stream on day 134 (Figure 1) prior to the sequence 1 stream. In Figure 3 the slow rise in speed of the sequence 1 stream starts near the end of day 135 and continues throughout day 138. *Dst* lies between ~-10 nT and -50 nT for these four days. This region of more or less continuous low-level *Dst* occurs both on the trailing edge of the precursor stream and on the leading edge of the larger sequence 1 corotating stream.

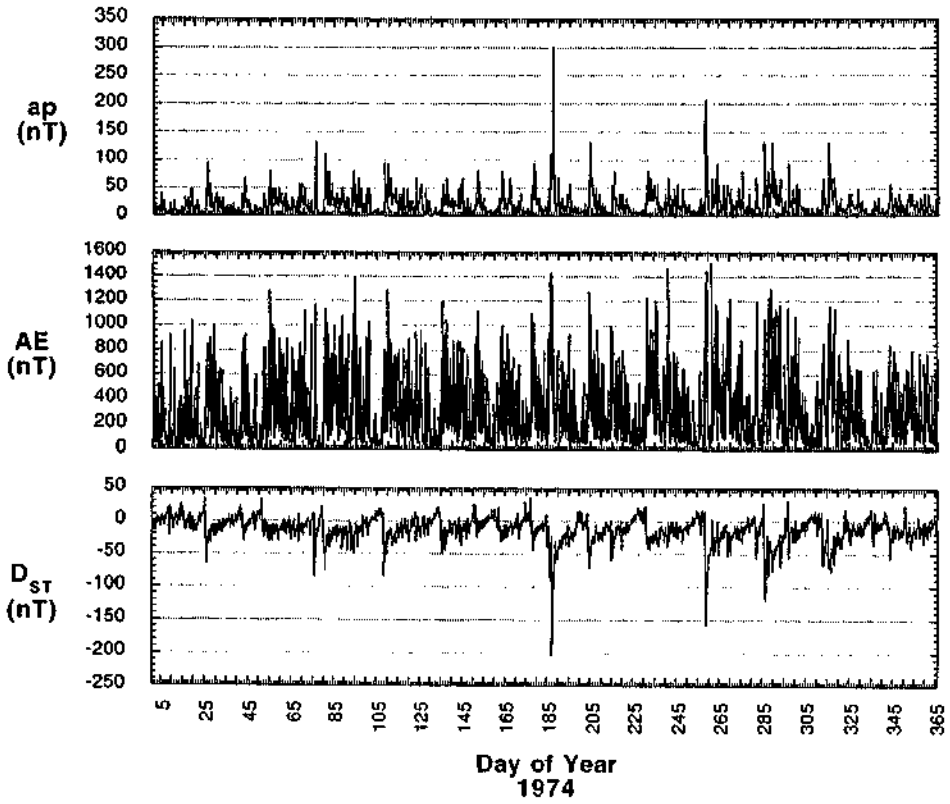

Figure 4. Hourly averages of *ap*, *AE* and *Dst* for 1974.

The causes of these small *Dst* decreases can be understood by examining simultaneous *AE* indices. There is almost a one-to-one correspondence between substorms (*AE*) and ring current increases (*Dst* decreases). Substorms are continuously occurring during this 4-day interval. Substorms cause the sporadic *Dst* decreases and prevent a full recovery of the ring current to quiet day values. This continuous *AE* activity is a high-intensity long-duration continuous *AE* activity (HILDCAA) event [*Tsurutani and Gonzalez*, 1987]. These substorms are caused by negative B_z components which are parts of large-amplitude Alfvén waves [*Tsurutani et al.*, 1990]. The Alfvén waves will be discussed later.

All of the other storm long recovery phase events are associated with HILDCAA events. These in turn are associated with large-amplitude Alfvén wave events where the wave components have significant negative B_z components. One possible interpretation of these results is that the B_z components of the Alfvén waves lead to magnetic reconnection and substorms, and these substorms lead to the injection of small amounts of particle energy into the outer regions of the magnetosphere where they decay rapidly. More on this topic will be stated in the following section.

Substorm (*AE*) Relationship to Storms (*Dst*)

Figure 4 gives the *ap* and *AE* indices for 1974 with the *Dst* index repeated as a reference. The *AE* and *Dst* indices are 1-hour values, and the *ap* indices are 3-hour values. As previously stated, the annual *AE* average is an exceptionally high value of 283 nT [*Saba*, 1992]. However, it can be noted that *AE* rarely attains (hourly average) intensities above 1200 nT. All cases of high *AE* events occur during relatively large magnetic storms. The *AE* > 1200 nT intervals are found on days 54 (~1200 nT), 94 (~1400 nT), 109 (~1300 nT), 186-187 (~1400 nT), 204 (~1200 nT), 231 (~1200 nT), 241 (~1400 nT), 259 (~1400 nT), 270 (~1200 nT), and 289-290 (~1300 nT). Events on days 186-187, 204, 231, and 288-289 occurred during storm main phases. On days 54, 109, 259, and 261 the peak *AE* events occurred during storm recovery phases. For the latter cases, significant ring current intensifications (*Dst* decreases) are associated with these *AE* events.

To answer the question, "If the peak *AE* values are not exceptionally large, then what is it that causes the average *AE* value for 1974 to be unusually high?", we compare the *AE* index to *Dst* for sequence 1. Starting on day 25, we note that *AE* reaches a peak intensity of ~800 nT within one-half day, corresponding quite closely to the *Dst* decrease in the storm main phase (day 25 is also shown in Figure 7; 2.5-min average *AE* values are used for this latter figure). However, *AE* remains quite high for many days afterward, up through day 31 and beyond. Throughout this period, *Dst* generally recovers, but there are frequent small ~10- to 20-nT decreases, indicating small ring current (energy) injections. The next occurrence of the high-speed stream is on day 53. *AE* oscillates between ~250 nT and ~1000 nT from day 53 through day 60. The solar wind speed declines from a peak value of ~750 km s^{-1} to ~600 km s^{-1} throughout this interval. *Dst* has values between -10 and -20 nT with no indication of decaying further. Again, frequent small *Dst* decreases are associated with *AE* increases.

The next passage of this sequence 1 high-speed stream occurs on days 79-80. A peak velocity of ~750 km s^{-1} is reached on day 80, and the stream speed decays to ~540 km s^{-1} by day 86. On day 79 there is a sharp increase in *AE* to peak values of ~1000 nT. This occurs concurrently with the storm main phase. *AE* remains high until day 86, when there is a sharp but short drop and then a return to high values.

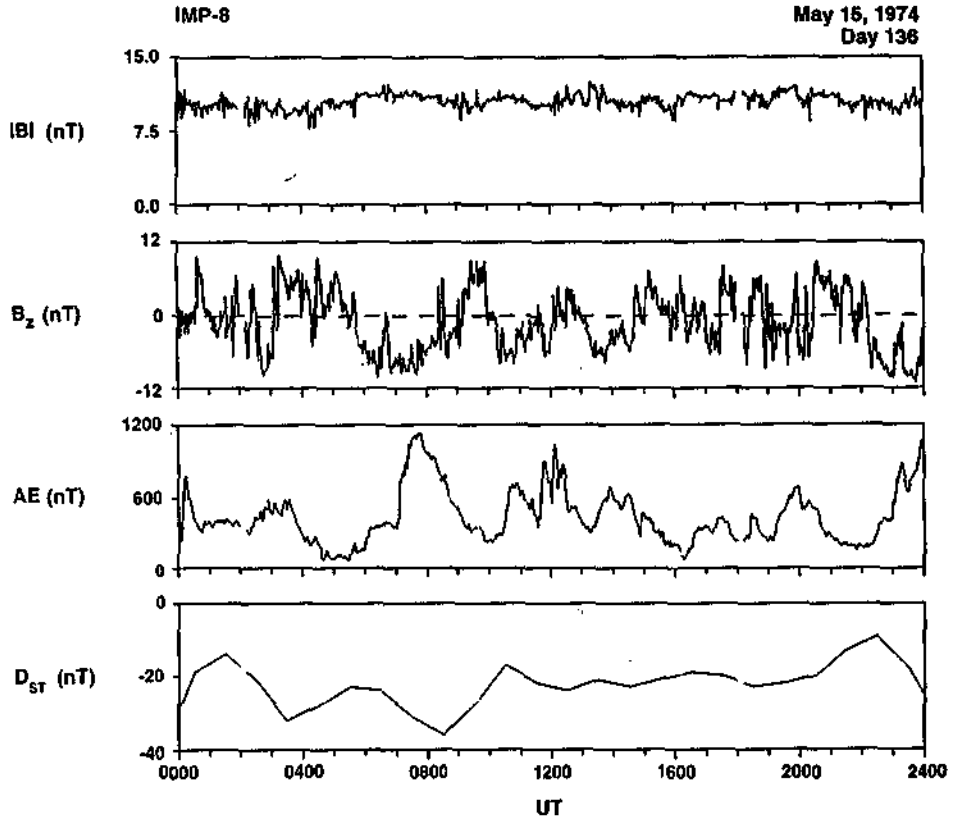

Figure 5. The IMF B magnitude, B_Z, AE and Dst for day 136, 1974. Increases in B_S and AE and slightly delayed increases in Dst are illustrated by this example.

The other appearances of the stream are similar to those discussed above. We skip to the last event where the stream speed and strength have decreased substantially. The eighth appearance of the stream occurs on day 214. On this day, AE abruptly increases to ~750 nT, decreases to 250 nT, and increases again to ~800 nT on day 215. Two Dst decreases correspond to these two AE events. AE remains relatively high (100 to 600 nT) through day 222, after which AE decreases below 200 nT. The solar wind speed decreases to <500 km s^{-1} after day 222. The association among V_{SW}, AE, and Dst is generally the same for stream sequence 2.

Interplanetary Alfvén Waves and HILDCAAs

What are the interplanetary feature(s) causing this AE activity? Figure 5 gives an example of the IMF B_z component in substantially higher time resolution. Also included in the figure are 2.5-min AE averages, B magnitude, and Dst. It can be noted from the B_z component of the field that the interplanetary magnetic field is highly turbulent. Some of these field fluctuations have large southward (B_S) values. A one-to-one correlation can be noted between B_z decreases and AE increases, indicating that magnetic reconnection is driving magnetospheric substorms on Earth. Because the B_S events associated with these fluctuations are not as intense and do not last as long as those associated with the storm main phase events, particularly for those of the A, B, and C events (here typically B_S ~-5 to -10 nT with durations of ~30 min to ~2 hours), the ring current particle injections caused by the Alfvén wave B_S events are not as substantial. Other periods have been examined with the same general findings.

A cross-correlation analysis of 24 hours of the plasma and magnetic field y components is given in Figure 6. At zero lag, V_y and B_y have a peak correlation coefficient of 0.65, indicating that these fluctuations are Alfvén waves propagating outward from the Sun [*Belcher and Davis*, 1971; *Tsurutani et al.*, 1990]. The southward deviations in the field associated with these waves are causing the high-latitude (auroral) geomagnetic activity through magnetic reconnection. Other 24-hour intervals where large-amplitude B_Z fluctuations were present were analyzed. We obtain

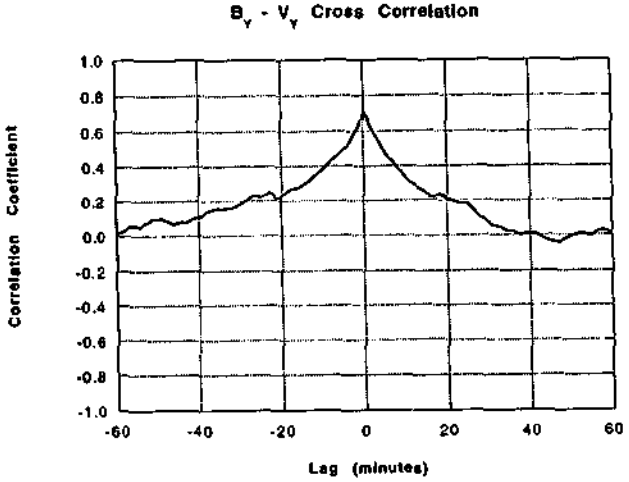

Figure 6. Cross correlation between the solar wind V_y and B_y for day 136, 1974. The peak correlation coefficient at zero lag indicates that the B_y and V_y fluctuations are Alfvén waves propagating outward from the Sun.

similar correlation coefficients peaked at zero lag. If the time intervals of analyses are shortened to 12 or 6 hours, the correlation coefficient increases to 0.8 or larger.

These relatively intense *AE* events presented here are similar to the HILDCAA events previously noted during solar maximum [*Tsurutani and Gonzalez*, 1987; *Tsurutani et al.*, 1990]. The only apparent difference is that the *AE* events discussed here do not necessarily fit the stringent requirements that the *AE* index remain above the 200-nT threshold for 48 hours and that *AE* < 200-nT intervals are less than 2 hours in duration. This somewhat arbitrary HILDCAA definition was/is artificial, and the important thing here is that more or less continuous auroral substorms (HILDCAAs) are produced by the B_S components of interplanetary Alfvén waves.

The cause of the strong *AE* activity during 1974 is the presence of the two high-speed corotating streams that contain large-amplitude Alfvén waves throughout the streams. The waves are almost continuously present, far more so than during solar maximum intervals. When this plasma and field impinge on the Earth's magnetosphere, the southward field turnings associated with the wave fluctuations cause magnetic reconnection and consequential high levels of *AE* activity. The waves appear to be most geoeffective when the solar wind speeds are near their maximum values. *AE* is found to decrease with decreasing solar wind speed, particularly when V_{SW} decreases below 500 km s^{-1}. Speed is probably not the only physical cause, however. The wave amplitudes are larger in the region of peak speed and generally decrease with decreasing speed.

Twenty-Seven-Day Periodic Quiet Geomagnetic Intervals

Intervals of geomagnetic quiet have been noted as well (see Figure 1). There are small intervals where *AE* is generally less than 200 nT for days at a time. These events are found in intervals that precede the onset of the high-speed corotating streams. Examples of events somewhat prior to the sequence 1 streams are found on days 22-24, 49-50, 77-78, 102-105, 130-133, and 224-227. Each of these intervals also partially overlaps with intervals where *Dst* is positive (discussed previously).

Four of the six low-*AE* events mentioned above have common interplanetary features. In these cases the velocities decrease from 560 to 310 km s^{-1}, 520 to 300, 460 to 360, and 400 to 360 (with a minimum of 300 km s^{-1}), respectively. The magnetic field magnitude ranges from 6 to 3 nT, 7 to 5, 6 to 8, and 5 to 3 nT during these intervals. The B_z component variability during these intervals was generally small. There is a general absence of Alfvén waves. There also may be a slight tendency for these intervals to have an average positive B_z value.

Several plasma features are generally consistent during the above four events. They occur within the far trailing portion of high-speed streams. The speeds start near 500 km s^{-1} and decrease with time. The temperatures also decrease and the plasma densities increase throughout the events. The densities start at values near the lowest detected in solar wind, ~3 cm^{-3}, and increase to substantial values (as the HCS is approached). For the five cases, *N* increases from 23 to 65 cm^{-3} (just prior to the stream onset and HCS crossing at the start of day 25), 3 to 12 cm^{-3} (including a broad HCS crossing from days 105-106), 3 to 11 cm^{-3} (just prior to a HCS crossing at the end of day 133), and 5 to 40 cm^{-3} (just prior to the HCS crossing at the beginning of day 231). The higher ram pressures associated with the enhanced interplanetary densities and the lack of ring current energy injections (due to the presence of relatively weak |*B*| without directional fluctuations) are the causes of the positive *Dst* values.

The two events that did not follow this general pattern are found on days 49-50 and 77-78. The first occurred in a low solar wind speed region, 340 to 430 km s^{-1}, just prior to the HCS crossing on day 51. The density was relatively high, 10 to 30 cm^{-3}. The magnetic field varied from 9 to 4 nT. All of these plasma and field features are similar to those occurring near the end of the previous five events. The only difference is that the event was not associated with a trailing portion of a high-speed stream. The magnetic field was also distinctly northward during this interval.

The final quiet event of the seven events, the event on days 77-78, is associated with a moderate speed impulsive stream which is located midway between a sequence 2 stream (onset on day 68) and a sequence 1 stream (onset at the end of day 79). The small stream creates a large magnetic magnitude compression on days 75-76 and a magnetic storm onset on day 75 associated with an intense B_S event at the front end of the stream. In the quiet interval the IMF magnitude decreases from 15 nT to 5 nT, and the density varies from 15 to 4 cm^{-3}. The HCS crossing occurs at the beginning of day 79, just after the geomagnetic quiet event. The main cause of this particular interval of geomagnetic quiet is that B_z is positive throughout the stream interval.

Twenty-Seven-Day Recurrence in *ap* Activity

The top panel in Figure 4 is the *ap* index. This index is constructed from midlatitude magnetometer stations. The index is sensitive to and therefore represents both ring current and auroral activity. By using *ap* alone, it is difficult/impossible to tell whether the activity is storm (*Dst*) activity or high-latitude substorm (*AE*) activity. The *ap* index is largest during the main phases of the largest storms. However, the index also picks up both the sequence 1 and sequence 2 corotating stream Alfvén wave-related events as well. There is a clear 27-day periodicity in this index. The 1973 and 1975 data contain similar features. The most intense *ap* intervals are those associated with impulsive streams (ejecta events), but there are clear 27-day periodicities associated with the coronal hole-associated streams as well. Thus if one examined *ap* indices alone, one could obtain the impression that there were intense 27-day recurring geomagnetic storms rather than 27-day recurring intense high-latitude auroral activity (there are recurring magnetic storms but they are low in intensity). From these 3 years of study there are no 27-day recurring intense (*Dst* ≤ -100 nT) magnetic storms.

Corotating Stream Case Studies

To illustrate the types of phenomena associated with southward B_z values that lead to the moderate *Dst* magnetic storms during 1974, we show two specific interplanetary corotating storm examples. We will examine our high-speed corotating stream events at the beginning of the sequence 1 streams and an event near the end of the sequence 2 streams.

Day 25

Prior to the beginning of the event illustrated (Figure 7), the field has exceptionally low values of ~1 nT at 1445-1700 UT on day 24 and has an orientation that is in neither a plus or minus sector polarity (see Figures 1 and 2). The solar wind has a low

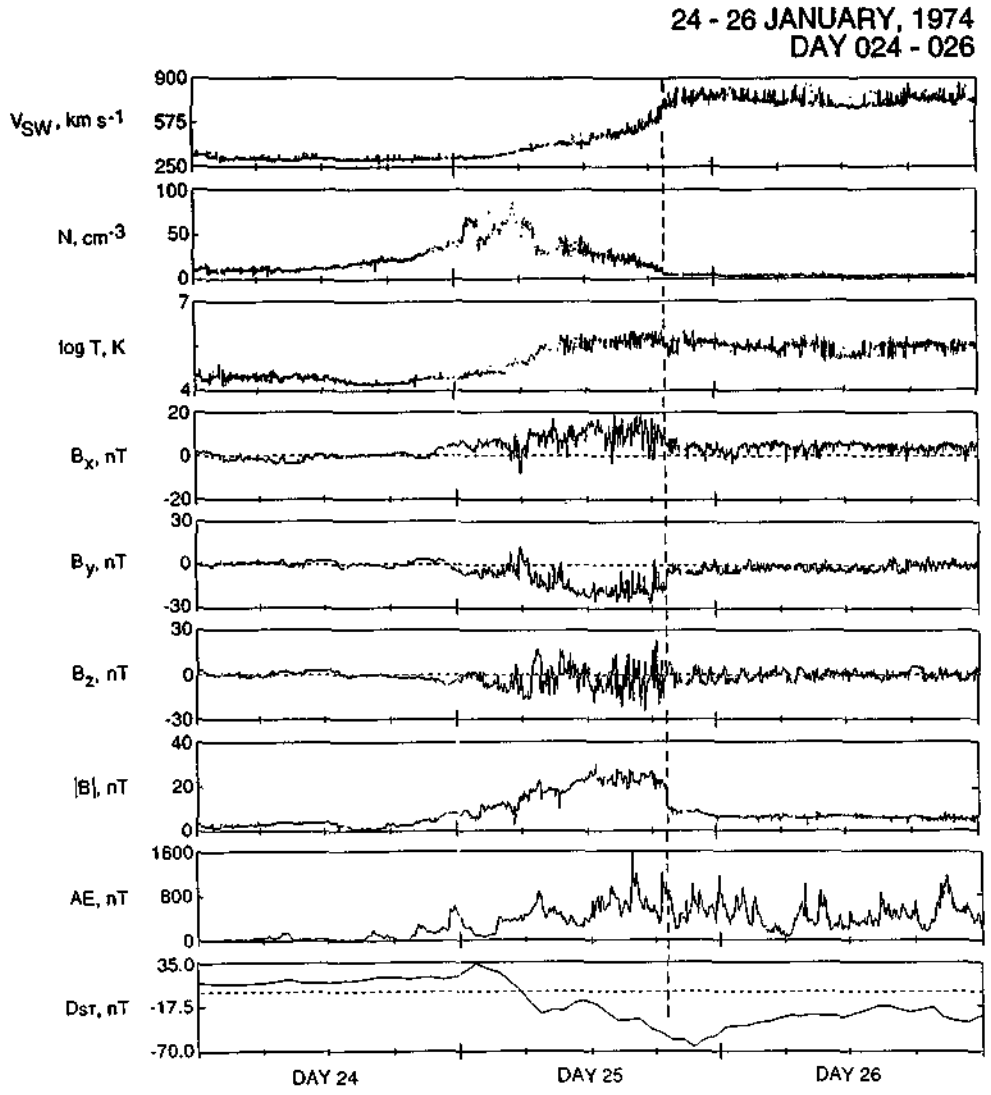

Figure 7. The *Dst* ~ -65 nT storm created by a corotating stream/heliospheric current sheet (HCS) interaction on day 25, 1974.

velocity (300-310 km s^{-1}) as well as a low proton temperature (~2 x 10^4 K). The plasma density is high, ~20-30 cm^{-3}, and causes positive *Dst* values. These plasma features give a good indication that the spacecraft (and Earth) is probably near the HCS [see *Winterhalter et al.*, 1994]. The low magnetic field strengths (and therefore low potential B_Z values) cause very low *AE* values, as discussed previously.

From 1700 UT on day 24 to 1200 UT on day 25 there are steady trends in several of the plasma parameters. The magnetic field increases from ~1 nT to 25 nT. *N* increases from 15 cm^{-3} to 80 cm^{-3} (at ~0500 UT) and then decreases to 30 cm^{-3}. There are no significant velocity and temperature gradients until ~ 0400 UT on day 25. At the beginning of this interval the solar wind speed starts at 330 km s^{-1} and rises, and the temperature starts at 3 x 10^4 K and rises. By 1200 UT, day 25, V_{sw} is ~450 km s^{-1} and *T* is ~5.5 x 10^5 K. The increasing plasma density leads to an increase in the solar wind ram pressure and hence a peak *Dst* of ~ + 35 nT at ~0200 UT on day 25.

Beyond 1200 UT on day 25 the velocity continues to increase, reaching a maximum of 775 km s^{-1} at ~1900 UT on day 25. The temperature reaches a maximum of ~6 x 10^5 K from 0800 to 1910 UT on day 25 and suddenly decreases to 4 x 10^5 K at 1910 UT. This abrupt decrease is due to the presence of a reverse shock, identified in the plasma and field parameters. The solar wind speed jumps from 620 km s^{-1} to 740 km s^{-1}, the density abruptly decreases from 12 to 5 cm^{-3}, and the magnetic field magnitude decreases from 22 to 10 nT. This example of a reverse shock occurring at 1 AU is fairly common (~20%) in the corotating streams studied. Note that the decrease in field magnitude is also accompanied by a decrease in B_S. The reverse shock causes a sharp decrease in B_s (in time) and starts the recovery phase of the storm. This is the opposite of the (forward) shock compression events causing storm onsets [*Tsurutani et al.*, 1988, and events A and B of this paper].

Although there is a clear reverse shock, there is no accompanying forward shock. This is contrary to the general picture presented by *Smith and Wolf* [1976], which has forward shocks occurring at ~1.5 AU and reverse shocks at ~2.5 AU. One speculation for the lack of a companion forward shock is the unusual plasma conditions upstream of the corotating stream (the HCS and its plasma sheet). The density is very high (up to 80 cm^{-3}) at this interaction region, and the magnetic field strength |B|

~25 nT is intense because of the stream-stream interaction. After 1300 UT on day 25, when the velocity gradient is steepest, the density is 20-25 cm^{-3} and decreasing. The field is a relatively constant ~25 nT. Thus the local Alfvén speed is 90 km s^{-1} at 1300 UT and increases with time. The solar wind speed is only 480 km s^{-1}, so the lack of a stronger velocity gradient and the relatively high Alfvén wave speed may prevent a forward shock from forming. See also discussion by *Belcher and Davis* [1971], *Hundhausen* [1973, 1985] and *Pizzo* [1985] for concepts/models of fast shock formation in the heliosphere.

The location of the HCS is somewhat difficult to place in this case. The IMF is clearly a negative sector polarity (positive B_x, negative B_y) after ~ 0000 UT on day 25. Prior to that time the polarity is mixed or is in an orthospiral (orthogonal to the normal Parker spiral) orientation. The largest plasma densities are on the same side of the HCS as the high-speed stream, possibly indicating that this may be compression due to the stream-stream interaction. However, it should be noted that the magnetic field intensification is found well behind the density enhancement.

The B_z that causes the storm is clearly related to the corotating stream interaction with the HCS and its plasma sheet. B_z steadily decreases from +3 nT at 1200 UT on day 24 to -10 nT at 0400 UT on day 25 as the HCS plasma sheet density increases from 12 to 60 cm^{-3}. The most intense B_s field during the event occurs from 0600 UT to 0655 UT on day 25 with a peak intensity of 16 nT. This intense southward IMF is coincident with the magnetic storm onset. The location of this B_s event is found at the base of the HCS plasma sheet/stream interface. The speed of the stream is only 370 km s^{-1} at the time.

It is noted that the B_s fluctuations causing the storm are parts of large-amplitude B_z variations. The origins of the intense B_z fluctuations are not presently known. They may be locally generated from stream-stream interaction effects, or they may be amplified Alfvén waves from the coronal hole stream. Tests are currently being run. We note that the field magnitude decrease across the reverse shock (in time) is a factor of ~2.5. We also note that the Alfvén wave transverse amplitudes decrease by a similar factor. This finding is suggestive that the latter hypothesis may be the correct one.

Recent Ulysses results are in accord with the suggestion that the above fluctuations are Alfvén waves. The Ulysses magnetic field and plasma results have indicated that polar coronal holes consist of a relatively steady high-speed stream of 750-800 km s^{-1} [*Phillips et al.*, 1994] with the presence of large-amplitude ($\Delta B/|B|$ ~1-2) Alfvén waves throughout the stream [*Tsurutani et al.*, 1994; *Smith et al.*, 1995]. Presumably, these are the same solar wind structures that reach the ecliptic plane during the descending phase of the solar cycle. The embedded fluctuations would then propagate/be convected into and become part of the stream-stream interaction region (up to the high-speed stream/low-speed stream interface, assuming it is a tangential discontinuity).

Day 177

The corotating stream event for days 176 through 179 is illustrated in Figure 8. At 1200 UT on day 176, well prior to the stream onset, V_{sw} is ~315 km s^{-1}, N is ~10 cm^{-3}, T is ~5 x 10^4 K, and $|B|$ is ~6 nT. At the very beginning of the stream gradient, ~0000-0600 UT on day 177, the density increases to 35-65 cm^{-3}. The increased solar wind ram pressure causes *Dst* to reach ~+35 nT during this interval. Since the solar wind speed increase is only slight, the *Dst* (ram pressure) increase is due almost entirely to the density enhancement.

The magnetic field magnitude also abruptly increases with the density increase. Peak values of ~25 nT are reached near ~0600 UT on day 177. However, somewhat different from the plasma density profile, the magnetic field intensity remains high until ~1500 UT on day 177. Thus the density enhancement is located at the very base of the corotating stream and the magnetic field enhancement further within the stream gradient. The corotating stream peak speed of 750-800 km s^{-1} is attained at ~0000 UT on day 178 when the field has decreased to a steady ~7 nT.

The location of the HCS can be noted by examining the IMF B_y and B_x components. Prior to ~0500-0600 UT on day 177, B_x is generally negative, and after that time, B_y is positive. There is a broad discontinuity from ~0500 to 0600 UT, when B_y reverses sign. Prior to ~0500 UT, B_x is positive, and after ~1000 UT, B_x is generally negative. Thus one can possibly interpret the ~0500 to 0600 UT interval as a crossing from a negative sector field to a positive sector field.

The largest and longest duration negative B_z event occurs at this transition. B_z has a value of ~ -15 nT for ~1 hour. This is coincident with the B_y sign reversal. The negative B_z event marks the start of the small storm (*Dst* ≤ -15 nT). The nature of the field within the high field region is again of a highly fluctuating nature. These fluctuations could be interpreted as amplified Alfvén waves. Subsequent negative B_z values on days 178-179, associated with Alfvén waves, lead to a peak *Dst* ~ -45 nT on day 178.

HCS Crossings and Geomagnetic Activity

We have examined all of the other magnetic storm events occurring during 1974 with *Dst* ≤ -50 nT. We wish to determine whether there is any dependence on the polarity of the IMF, a dependence that might be present if the equinoctial hypothesis is the predominant cause of these smaller storms [*Russell and McPherron*, 1973; *Crooker et al.*, 1992a], (however, see discussion by *Gonzalez et al.* [1993]). We have also examined the data for possible storm seasonal dependences. There are fourteen *Dst* ≤ -50 nT events in all. Seven of these are associated with HCS +/- crossings and seven are associated with -/+ crossings. Thus there is no obvious HCS crossing polarity dependence. Although there is no HCS crossing dependence, there is some evidence that negative sectors within March-April and positive sectors within September-October tend to favor *Dst* enhancement, in agreement with the Russell-McPherron mechanism. This slight effect can be seen in Figure 1.

Major Storm (*Dst* ≤ -100 nT) Case Studies

Event A

The "A" event was the largest magnetic storm that occurred during 1974. It can be noticed in Figure 1 that the stream(s) responsible for the storm do(es) not occur either 27 days before or after. In the figure it can be noted that the storm is composed of three distinct main phase components, each main phase more intense than the previous one. These main phases are related to three separate streams, each led by fast-forward shocks. Each stream is nonrecurring rather than corotating.

In Figure 9 we show the high-resolution B_z, $|B|$, speed, density, and temperature values for the A event from 1200 UT on day 185

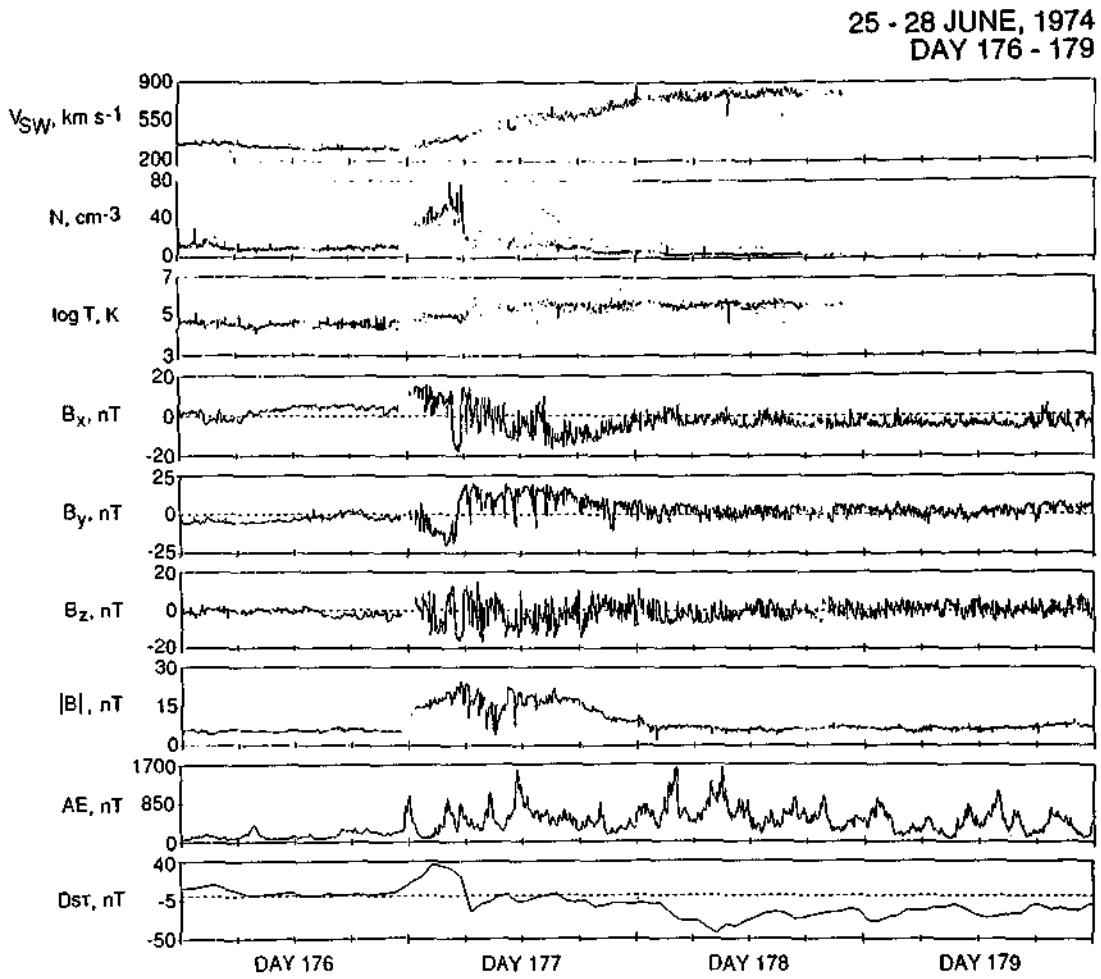

Figure 8. A *Dst* ~ -45 nT magnetic storm created by a corotating stream/HCS plasma sheet interaction on days 177-178.

until 2400 UT on day 187. The first fast-forward shock occurs at 0109 UT on day 185 (not shown). The magnetic field compression associated with this shock crossing was relatively small owing to the low stream speed of only 490 km s^{-1}. Figure 9 shows the second forward shock at 1532 UT on day 185 (indicated by a dashed vertical line). The peak stream speed is again only ~490 km s^{-1}. The magnetic field magnitude increases from ~9 nT to 15 nT across the shock. Well behind the shock at 2245 UT there is a sharp IMF discontinuity in which the field changes from a northward value to one directed southward. The B_s component becomes ~9 to 12 nT and remains at this value throughout the stream. A peak *Dst* value of -85 nT develops at 0700 UT, day 186. The most intense main phase onset is related to the third, higher-speed ejecta. The speed increases from an upstream value of ~450 km s^{-1} to a postshock speed of 600 km s^{-1}. B_s increases from a value of 10 nT upstream to over ~25 nT downstream. The cause of the intense B_s event that causes the storm is shock compression of preexisting upstream B_s fields.

From 0410 UT until 0640 UT, day 187, the density is in the range of ~35 cm^{-3}, and the temperature is ~2 x 10^5 K (not shown). The high plasma densities and temperatures do not fit with the possibility of this being part of the driver gas for the event.

Event B

This interplanetary event is another nonrecurring event led by an interplanetary shock (see Figure 1). The event is shown in high resolution in Figure 10. The storm sharp onset is again caused by shock compression of preexisting southward fields. The B_z field is ~ -15 nT prior to the shock (causing a decrease in *Dst*), becomes compressed to <-40 nT at the shock at 1350 UT on day 258, and remains at high negative values until 1432 UT. B_z then oscillates between +5 nT and -40 nT until 1622 UT, when it remains at -40 nT. B_z then maintains a -40 to -50-nT level until 1830 UT on day 258.

We have searched for a classical driver gas, using most of the *Zwickl et al.* [1983] criteria (low temperatures, enhanced He abundances, and quiet magnetic fields), but have not found an obvious region. The fields between 1830 and 2400 UT, day 258, are large and somewhat devoid of waves. The interval has low plasma densities (1-5 cm^{-3}) as well. However, the temperature remains high (~6-8 x 10^5 K) throughout this region, contrary to the *Zwickl et al.* criteria for a driver gas. Although it is possible that this may be a driver gas (without all *Zwickl et al.* criteria met), it is not the major cause of the B_s event responsible for the storm main phase and does not warrant further study within this paper.

What is the cause of the highly turbulent fields within the above B_z event? The answer can be found by looking at the other field components and the field magnitude. Prior to the shock passage, the IMF is in the orthospiral direction with large negative B_y (~ -10 nT) and an even larger negative B_z (-15 to -20 nT) component. In the interval (1432 to 1622 UT) when B_z varies from +5 nT to -40 nT, B_x is large and positive (20 to 30 nT), and

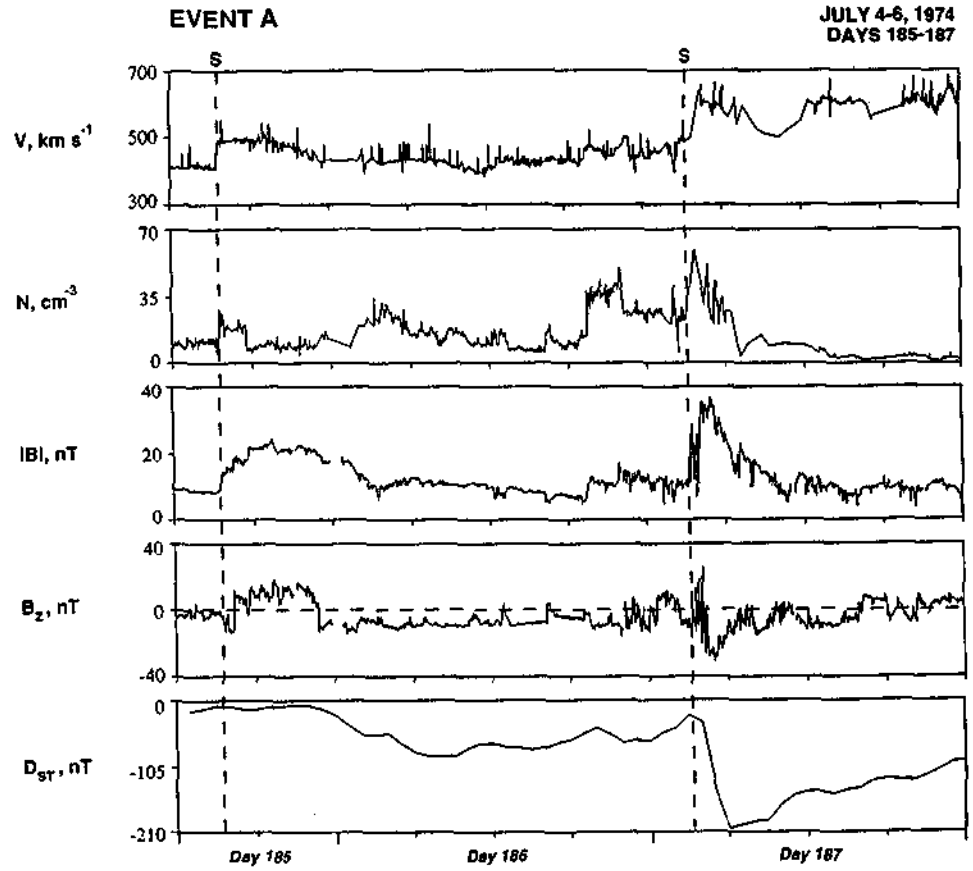

Figure 9. Two of the streams and shocks responsible for the day 185-187 complex magnetic storm (the A event). The solar wind speed, density, magnetic field magnitude, and B_z component are displayed. Hourly average *Dst* is given in the bottom panel.

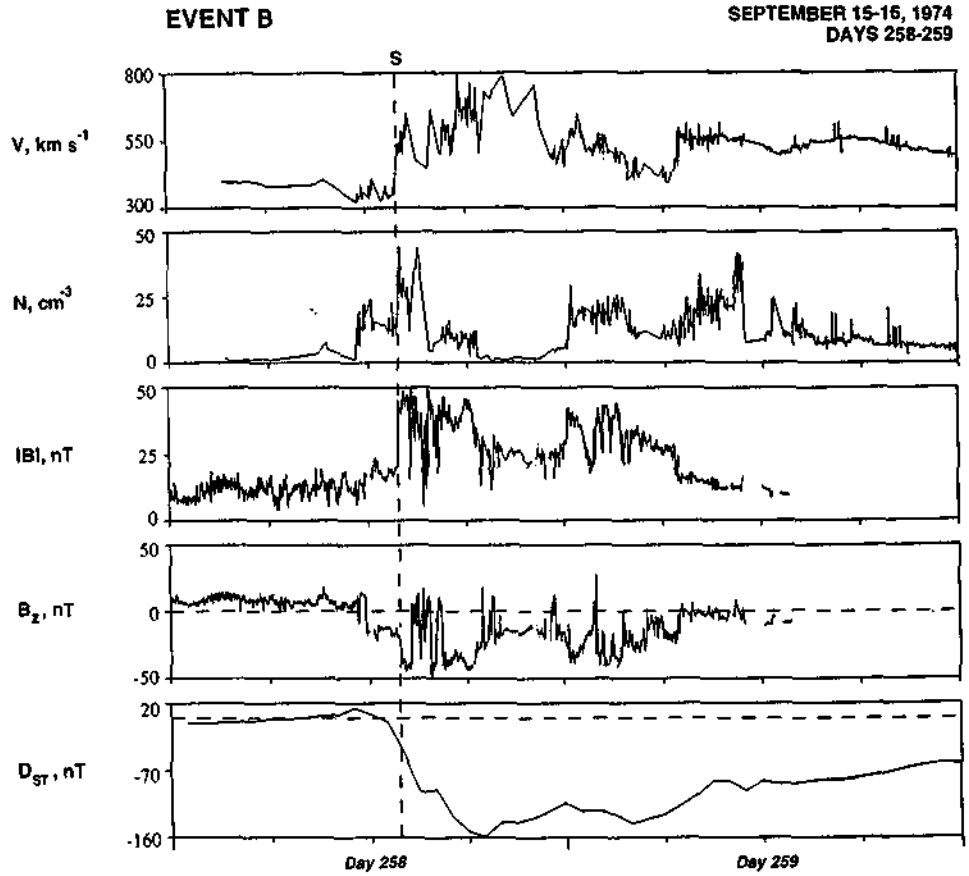

Figure 10. The B storm event. The B_S event responsible for the storm is created by shock compression of upstream B_S fields.

B_y is positive (0 to 10 nT) but less intense than B_X. There are also large magnetic field magnitude decreases associated with the field directional changes, indicative of the presence of strong local currents. After the field fluctuation region, from 1622 UT and later, the B_x and B_y fields are well ordered, with values of -10 nT and +10 nT, respectively. This is a positive sector field orientation. Thus one possible interpretation of the field fluctuations between 1432 and 1622 UT is that this is a multiple crossing of the heliospheric current sheet or the crossing of several separate current sheets [*Crooker et al.*, 1992b]. Prior to the high-speed event the plasma density is high and the velocity low (not shown), indicating an approach to the HCS region. The clear orientation of the field afterward is perhaps the strongest evidence for the hypothesis of a current sheet crossing.

Event C

The third most intense storm during 1974 is again associated with a nonrecurring stream led by a fast-forward shock (Figure 11). The shock event occurs at 1245 UT on day 285, when the magnetic field magnitude increases from 5 nT to ~12 nT, the solar wind speed from 400 to 500 km s^{-1}, and density from ~10 to ~20 cm^{-3}. Shock compression of the interplanetary fields increases B_z from +5 nT to +12 nT. The initial phase of the storm (positive *Dst* values) starts with the shock passage and associated high solar wind ram pressure.

The southward IMF responsible for the storm is associated with the driver gas fields. This is clearly denoted by the smooth magnetic fields detected at 2100 UT extending to 0135 UT on day 287 (the full extent is not shown). The fields are large and smooth with little wave activity and essentially no discontinuities (of all of the criteria used to identify the driver gas this is one of the best presently available; however, no one measure works 100% of the time). This is consistent with the standard picture of a magnetic cloud [*Burlaga et al.*, 1987] within a driver gas [*Zwickl et al.*, 1983; *Tsurutani et al.*, 1988; for a discussion of the relationship among magnetic clouds, CMEs and driver gases, see *Tsurutani and Gonzalez*, 1995a]. The magnetic field B_z decreases to -15 nT at ~0200 UT, day 286, and remains at this large value until 1400 UT on day 286. Near the end of the magnetic cloud at 0130 UT on day 287 the B_z component rises to +5 nT.

All three interplanetary events are ejecta events. Event A was caused by three superposed streams. Event B is an ejecta event which occurs where the corotating streams begin to become quite complex (as mentioned previously). Event C is due to a stream whose peak speed is less than 530 km s^{-1}. This latter event has a clean profile of a fast rise-slow decay signature and is impulsive in nature.

Solar Sources of the A, B, C Interplanetary Events?

Possible solar sources for the three high-speed streams (A, B, C events) were sought by examining the Solar-Geophysical Data (Boulder, Colorado) and the World Data Center A for Solar-Terrestrial Physics, report UAG-52, 1974. The speeds of the high-speed streams at 1 AU were also used to rule out events that would require unreasonably high or unreasonably low transit speeds.

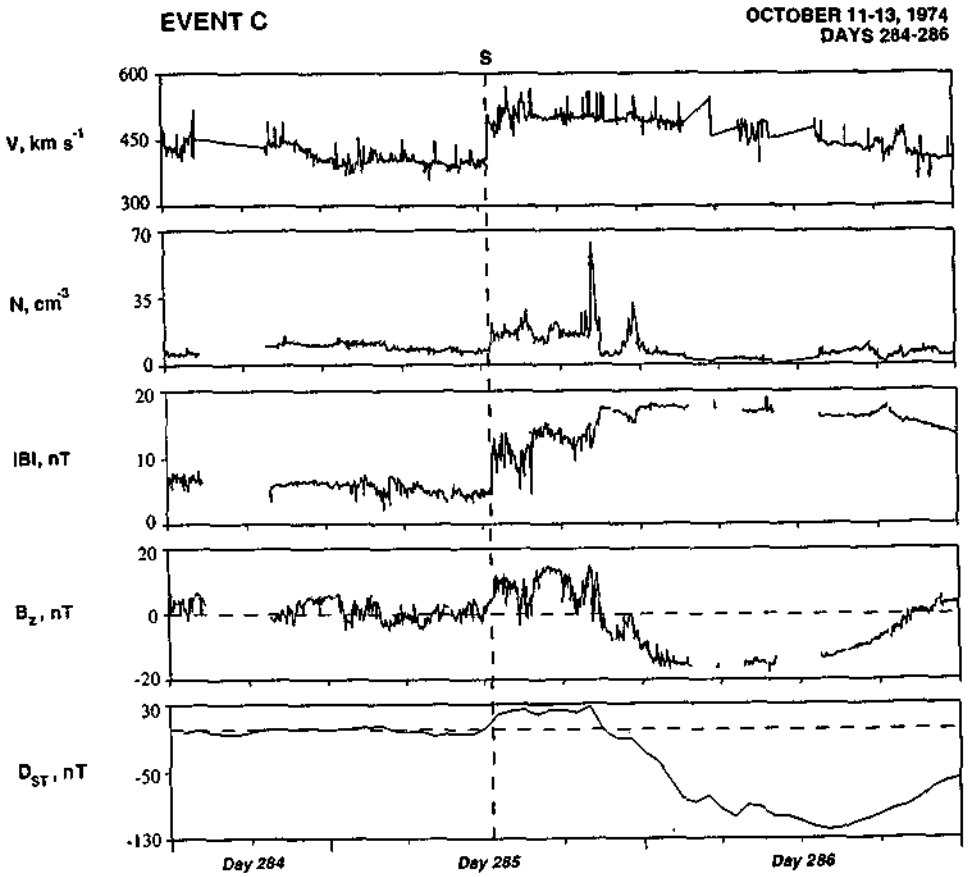

Figure 11. The C storm event. The storm is created by B_S within the driver gas (a magnetic cloud).

Event A

Three small 1B/2B flares were the most intense events during this period region (region 13043, day 184, 0259-0318-0412 UT, day 185, 0801-0840-0928 UT, and 1338-1357-1442 UT). Because event A is a compound event involving three interplanetary shocks, one might hope that these three flares would correspond to the three interplanetary shocks at 1 AU. However, the timing for the first two flares was within 24 hours of the detection of the shocks at 1 AU. Such unreasonably short transit times rule out these flares as possible sources, unless one assumes that very large deceleration is occurring between the sun and 1 AU.

The solar flare event at 0259 UT on day 184 is the only event that fits any of the three shocks time-wise. If one considers the last shock occurring at ~0000 UT on day 187, an average speed of ~604 km s^{-1} is determined. This is in good agreement with the measured postshock flow speed of ~600 km s^{-1}. However, no solar events could be related to the other two solar wind streams. The latter two are more important in terms of producing the geomagnetic storm. This event can be thought of as a compound stream, as discussed by *Burlaga et al.* [1987].

Event B

The interplanetary shock is detected at 1350 UT on day 258. The postshock flow speed is ~645 km s^{-1}. Assuming a constant flow from the Sun to the Earth, this would correspond to a transit time of ~2.7 days. The only obvious solar event during this time is a 2B flare on September 13. If this solar event is the cause of the interplanetary ejecta, the ejecta would have to have had an average transit speed of ~850 km s^{-1}. This is quite high considering the measured speed at 1 AU. This solar event seems like an unlikely candidate. There were no prominence disappearance events during the interval of interest.

Event C

The shock was detected at 1 AU at 1245 UT on day 285. The only prominent flare that occurred within the general time interval was on day 284 at 0325 UT. There were no prominence disappearance events in the interval of interest. The 2B flare occurred less than a day and a half prior to the detection of the shock at 1 AU. Because the stream speed was quite low, ~500 km s^{-1}, this solar event seems unlikely to be related to the storm-causing stream.

It has been extremely difficult to identify solar events associated with the A, B, and C storm-causing solar wind streams detected at 1 AU. These three nonrecurring events probably did not have optical or X ray counterparts.

Summary and Discussion

1. In 1974, only moderate (-100 nT ≤ *Dst* ≤ -50 nT), weak (-50 nT ≤ *Dst* ≤ -25 nT), or negligible (-25 nT ≤ *Dst*) magnetic storms were caused by corotating streams. Corotating streams were not responsible for major (*Dst* ≤ -100 nT) magnetic storms. Although the fast stream-slow stream interactions (corotating stream/HCS plasma sheet interactions) created intense fields with hourly average |*B*| ~15-25 nT and B_Z ≤ -10 nT, the B_Z component was typically highly fluctuating. The *Gonzalez and Tsurutani* [1987] criteria for a major (*Dst* ≤ -100 nT) magnetic storm (during solar maximum), a dawn-to-dusk E_{sw} ≥ 5 mV/m (approximately comparable to B_S ≤ -10 nT) and T > 3 hours, were not met at any of the corotating stream compression regions. The B_S value was often greater than 10 nT, but the time duration was less than 3 hours. Thus it is possible that this empirical criterion derived from a solar maximum interval, may also hold during the descending phase of the solar cycle as well. Similar results were found for 1973 and 1975 as well (not shown).

2. The extremely high annual 2.5-min *AE* average of 283 nT for 1974 was due to the presence of two corotating streams that contained continuous, large-amplitude Alfvén waves. As the magnetic field of the wave rotates southward, magnetic reconnection takes place at the Earth's magnetosphere, and a substorm occurs. As the field rotates northward, it turns off reconnection, and the substorm terminates. The quasi-periodic southward components cause the quasi-periodic substorm activity, called HILDCAAs.

3. The magnetic storms caused by the corotating coronal hole streams have extremely long decay times, sometimes greater than ~10 days, even weeks. These are caused by the presence of HILDCAAs within the recovery phase. Substorms comprising the HILDCAAs inject small amounts of ring current particle energy into the outer regions of the magnetosphere that are detected as slight *Dst* decreases. The continuous substorms (and particle injections) tend to keep the ring current at a quasi-steady state and do not allow it to recover to its quiet time value. The relatively rapid 2- to 3-hour decay of these small *Dst* events is unexplained at this time, however. One possible explanation is that the particles gradient drift to the magnetopause and are convected into the magnetosheath. Another possibility is the IMF B_N part of the Alfvén wave may play a role in outward radial convection of the nightside ring current. A third possibility is that rapid particle loss to the auroral ionosphere caused by wave-particle interactions is occurring.

4. Intervals of geomagnetic quiet are associated with the far trailing portion of corotating streams where |*B*| is low (<3 nT) and there is an absence of Alfvénic fluctuations.

5. The physical mechanism for the "initial" (positive *Dst*) phases of magnetic storms is considerably different from that for fast ejecta events. For corotating streams it is the HCS plasma sheet and the stream-stream compressive effects that lead to the high solar wind plasma densities. These density enhancements can occur well ahead of high |*B*| intensities, and thus long-duration, purely positive *Dst* events result. Although the solar wind speeds in these regions are generally quite low, ~300-350 km s^{-1}, the densities are often an order of magnitude larger than average values, allowing significant ram pressure increases and the storm initial phase.

6. The three major (*Dst* ≤ -100 nT) magnetic storms that occurred in 1974 were not created by the corotating streams. All three were associated with moderate speed streams led by fast-forward shocks. The streams were not particularly notable (the highest had a speed of ~600 km s^{-1}), and all were located near the HCS crossings. One speculation that we propose is that these relatively smallish events might be related to the coronal hole expansion, i.e., the opening of additional magnetic flux in the corona. It was not possible to find any (small) solar flares or prominence eruptions associated with the interplanetary events.

7. Reverse shocks are present in corotating streams at 1 AU about ~20% of the time. They are not accompanied by forward shocks. If the prior fields had a southward direction, the decrease in magnetic field magnitude that occurs with a reverse shock

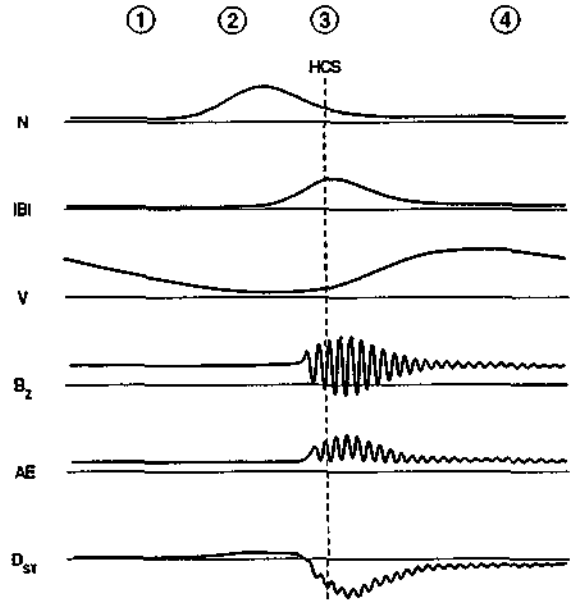

Figure 12. A schematic of the solar wind causes of geomagnetic quiet, small to moderate magnetic storms, and HILDCAAs during the descending phase of the solar cycle.

crossing (from downstream to upstream in time) causes the onset of the storm recovery phase.

8. The causes of the B_S events responsible for the A, B, and C magnetic storms were shock compression of preexisting southward B_Z for the two largest storm events and B_S within a magnetic cloud for the weakest event.

A schematic of geomagnetic active and geomagnetic quiet intervals summarizing the above results is given in Figure 12. Region 1 is the distant trailing portion of a high-speed stream. The speed is relatively low and is decreasing with time. The magnetic field magnitude is low and devoid of large-amplitude Alfvén waves. This is a region where *AE* is lowest (other than times when B_Z is northward for long intervals of time; see *Tsurutani and Gonzalez* [1995b]. In region 2 the plasma density is high owing to the presence of naturally occurring high densities near the HCS (the HCS plasma sheet) and also to stream-stream compressive effects. This region, when incident upon the magnetosphere, leads to positive *Dst* values. After the passage of this density enhancement, if the subsequent IMF has significant southward components causing a storm main phase, then the prior positive *Dst* will appear as a storm initial phase (without a sudden commencement). If there are no trailing southwardly directed fields, the former will only be a positive *Dst* event. Region 3 contains the high-intensity magnetic fields associated with stream-stream compressive effects. Southward deflections of the IMF lead to small or moderate magnetic storms. Note that at 1 AU this high field region is located at the beginning of the gradient of the high-speed stream and is not near the region where the gradient or velocity is the highest. This is considerably different from what happens with storms that occur during solar maximum (for shock compression of B_S this occurs at high-speeds just behind the forward shock; for magnetic clouds this occurs near the peak ejecta speeds). Because the fields in the interaction region are highly fluctuating, the storm main phases are also highly irregular in profile. Region 4, at the peak and trailing portions of the high-speed stream, is characterized by Alfvénic fluctuations in B_Z and concomitant continuous auroral activity (*HILDCAAs*). The *AE* intensity is highest near the peak of the stream and decreases with decreasing solar wind speed and Alfvén wave amplitudes. Recent Ulysses high-latitude results have given us additional information which help put these in-ecliptic observations/results into context. *Phillips et al.* [1994] have shown that the solar wind associated with polar coronal holes has constant speeds near 750-800 km s^{-1}. *Tsurutani et al.* [1994] and *Smith et al.* [1995] have shown that Alfvén fluctuations within such streams have continuous transverse fluctuations with $\Delta B/|B| \sim 1$ to 2. Thus the most intense HILDCAAs are associated with cases in which the coronal hole stream proper impinges on the magnetosphere. Trailing portions of the streams (rarefaction regions) have lower Alfvénic wave amplitudes and thus are less geoeffective, consistent with the above observations.

Why does the idea of 27-day recurring magnetic storms persist? At the time of the *Chapman and Bartels* [1940] book, only midlatitude indices such as *ap* were available. From these indices, one could not tell whether the geomagnetic activity was due to storms or substorms. From this study we clearly show that both are present. However, we note that the dominant cause of *ap* periodicity is the long-duration auroral activity (HILDCAAs) throughout the corotating stream.

Acknowledgments. Portions of this work were done at the Jet Propulsion Laboratory, California Institute of Technology, Pasadena, under contract with the National Aeronautics and Space Administration. We wish to acknowledge helpful scientific discussions with E. J. Smith. This paper was submitted simultaneously with that of Crooker and Cliver (*99*, 23383, 1994). The Editors (B. Hultqvist and T. Gombosi),who have read both, feel that they should be viewed as complementary in nature. The authors would like to thank the referees for their constructive comments.

The Editor thanks two referees for their assistance in evaluating this paper.

References

Bartels, J., Some problems of terrestrial magnetism and electricity in *Terrestrial Magnetism and Atmospheric Electricity* , edited by J. A. Flemming, p. 385, McGraw-Hill, New York, 1938.

Belcher, J. W., and L. Davis Jr., Large-amplitude Alfvén waves in the interplanetary medium, 2, *J. Geophys. Res., 76*, 3534, 1971.

Borrini, G., J. T. Gosling, S. J. Bame, W. C. Feldman, and J. M. Wilcox, Solar wind helium and hydrogen structure near the heliosphere current sheet: A signal of coronal structures at 1 AU, *J. Geophys. Res., 86*, 4565, 1981.

Burlaga, L. F., and R. P. Lepping, The causes of recurrent geomagnetic storms, *Planet. Space Sci., 25*, 1151, 1977.

Burlaga, L. F., K. W. Behannon, S. F. Hansen, G. W. Pneumann, and W. C. Feldman, Sources of magnetic fields in recurrent interplanetary streams, *J. Geophys. Res., 83*, 4177, 1978.

Burlaga, L., E. Sittler, F. Mariani, and R. Schwenn, Magnetic loop behind an interplanetary shock: Voyagers, Helios, and IMP 8 observations, *J. Geophys. Res., 86*, 6673, 1981.

Burlaga, L. F., K. W. Behannon, and L. W. Klein, Compound streams, magnetic clouds, and major geomagnetic storms, *J. Geophys. Res., 92*, 5725, 1987.

Chapman, S., and J. Bartels, *Geomagnetism*, vol. 1, chap. XII, 396, Clarendon, Oxford, England, 1940.

Crooker, N. U., E. W. Cliver, and B. T. Tsurutani, The semiannual variation of great geomagnetic storms and the postshock Russell-McPherron effect preceding coronal mass ejecta, *Geophys. Res. Lett., 19*, 429, 1992a.

Crooker, N. U., G. L. Siscoe, S. Shodhan, D. F. Webb, J. T. Gosling, and E. J. Smith, Multiple heliospheric current sheets and coronal stream belt dynamics, *J. Geophys. Res., 98*, 9371, 1992b.

Dessler, A. J., and J. A. Fejer, Interpretation of *Kp* index and *M*-region geomagnetic storms, *Planet. Space Sci., 11*, 505, 1963.

Dungey, J. W., Interplanetary magnetic field and the auroral zones, *Phys. Res. Lett., 6*, 47, 1961.

Farrugia, C. J., L. F. Burlaga, V. A. Osherovich, I. G. Richardson, M. P. Freeman, R. P. Lepping, and A. J. Lazarus, A study of an expanding interplanetary magnetic cloud and interaction with the Earth's magnetosphere: The interplanetary aspect, *J. Geophys. Res., 98*, 7621, 1993a.

Farrugia, C. J., M. P. Freeman, L. F. Burlaga, R. P. Lepping, and K. Takahashi, The Earth's magnetosphere under continued forcing: Substorm activity during the passage of an interplanetary magnetic cloud, *J. Geophys. Res., 98*, 7657, 1993b.

Feynman, J., and X. Y. Gu, Prediction of geomagnetic activity on time scales of one to ten years, *Rev. Geophys., 24*, 650, 1986.

Gonzalez, W. D., and B. T. Tsurutani, Criteria of interplanetary parameters causing intense magnetic storms (*Dst* < -100 nT), *Planet. Space Sci. 35*, 1101, 1987.

Gonzalez, W. D., and B. T. Tsurutani, Terrestrial response to eruptive solar flares: Geomagnetic storms, in *Eruptive Solar Flares*, edited by Z. Svestka, B. V. Jackson, and M. E. Machado, p. 277, Springer-Verlag, New York, 1992.

Gonzalez, W. D., and B. T. Tsurutani, Interplanetary-magnetosphere coupling from ISEE-3, in *Proc. Sol. Terr. Energy Prog. (STEP) Symp.*, edited by D. N. Baker, V. O. Papitashivili and M. J. Teague, *p. 435, Pergammon*, New York, 1994.

Gonzalez, W. D., B. T. Tsurutani, A. L. C. Gonzalez, E. J. Smith, F. Tang, and S. I. Akasofu, Solar wind-magnetosphere coupling during intense magnetic storms (1978-1979), *J. Geophys. Res., 94*, 8835, 1989.

Gonzalez, W. D., A. L. C. Gonzalez, and B. T. Tsurutani, Comment on "The semiannual variation of great geomagnetic storms and the postshock Russell-McPherron effect preceding coronal mass ejecta," *Geophys. Res. Lett.., 20*, 1659, 1993.

Gonzalez, W. D., J. A. Joselyn, Y. Kamide, H. W. Kroehl, G. Rostoker, B. T. Tsurutani , and V. M. Vasyliunas, What is a geomagnetic storm?, *J. Geophys. Res., 99*, 5771, 1994.

Gosling, J. T., J. R. Asbridge, S. J. Bame, and W. C. Feldman, Solar wind speed variations: 1962, *J. Geophys. Res., 81*, 5061, 1976.

Gosling, J. T., S. J. Bame, D. J. McComas, and J. L. Phillips, Coronal mass ejections and large geomagnetic storms, *Geophys. Res. Lett. 17*, 901, 1990.

Gosling, J. T., D. J. McComas, J. L. Phillips, and S. J. Bame, Geomagnetic activity associated with Earth passage of interplanetary shock disturbances and coronal mass ejections, *J. Geophys. Res., 96*, 7831, 1991.

Hansen, R. T., S. F. Hansen, and C. Sawyer, Long-lived coronal structures and recurrent geomagnetic patterns in 1974, *Planet. Space Sci., 24*, 381, 1976.

Hoeksema, J. T., and X. Zhao, Prediction of magnetic orientation in driver gas associated B_z events, *J. Geophys. Res., 97*, 3151, 1992.

Hundhausen, A. J., Evolution of large-scale solar wind structures beyond 1 AU, *J. Geophys. Res., 78*, 2035, 1973.

Hundhausen, A. J., Some macroscopic properties of shock waves in the heliosphere, in *Collisionless Shocks in the Heliosphere: A Tutorial Review*, edited by R. G. Stone and B. T. Tsurutani, *Geophys. Monogr. Ser., vol.. 34, p. 37*, AGU, Washington, D. C., 1985.

Klein, L. W., and L. F. Burlaga, Interplanetary magnetic clouds at 1 AU, *J. Geophys. Res., 87*, 613, 1982.

Krieger, A. S., A. F. Timothy, and E. C. Roelof, A coronal hole and its identification as the source of a high velocity solar wind, *Sol. Phys., 29*, 505, 1973.

Krieger, A. S., A. F. Timothy, G. S. Vaiana, A. J. Lazarus, and J. D. Sullivan, X ray observations of coronal holes and their relationship to high velocity solar wind streams, in *Solar Wind Three*, edited by C. T. Russell, p. 132, Inst. of Geophys. and Planet. Phys., Univ. of Calif., 1974.

Lindblad, B. A., Coronal sources of high-speed plasma streams in the solar wind during the declining phase of solar cycle 20, *Astrophys. Space Sci., 170*, 55, 1990.

Lindblad, B. A., and H. Lundstedt, A catalogue of high-speed plasma streams in the solar wind 1975-1978, *Sol. Phys., 88*, 377, 1983.

Ness, N. F., and J. M. Wilcox, Solar origin of the interplanetary magnetic field, *Phys. Rev. Lett., 13*, 461, 1964.

Neugebauer, M., and C. W. Snyder, Mariner 2 observations of the solar wind, *J. Geophys. Res., 71*, 4469, 1966.

Phillips, J. L., A. Balogh, S. J. Bame, et al., Ulysses at 50° south: Constant immersion in the high space solar wind, *Geophys. Res. Lett., 21*, 1105, 1994.

Pizzo, V. J., Interplanetary shocks on the large scale: A retrospective on the last decade's theoretical efforts, in *Collisionless Shocks in the Heliospheric Review of Current Research*, edited by B. T. Tsurutani and R. G. Stone, *Geophys. Monogr. Ser., vol., 35, p. 51, AGU*, Washington, D. C., 1985.

Russell, C. T., and R. L. McPherron, Semiannual variation of geomagnetic activity, *J. Geophys. Res., 78*, 92, 1973.

Saba, M. M., Intercomparison of the *AE*, *ap* and *Dst* indices for years near solar maximum (1979) and solar minimum (1974), M.Sc. thesis, Natl. Inst. of Space Res., Sao Jose dos Campos, Sao Paulo, Brazil, 1992.

Sckopke, N., A general relation between the energy of trapped particles and the disturbance field near the Earth, *J. Geophys. Res., 71*, 3125, 1966.

Sheeley, N. R., Jr., J. W. Harvey, and W. C. Feldman, Coronal holes, solar wind streams and recurrent geomagnetic disturbances: 1973-1976, *Sol. Phys., 49*, 271, 1976.

Sheeley, N. R., Jr., J. R. Asbridge, S. J. Bame, and J. W. Harvey, A pictorial comparison of interplanetary magnetic field polarity, solar wind speed, and geomagnetic disturbance index during the sunspot cycle, *Sol. Phys., 52*, 485, 1977.

Smith, E. J., and J. H. Wolfe, Observations of interaction regions and corotating shocks between one and five AU: Pioneers 10 and 11, *Geophys. Res. Lett., 3*, 137, 1976.

Smith, E. J., B. T. Tsurutani, and R. L. Rosenberg, Observations of the interplanetary sector structure up to heliospheric latitudes of 16 degrees: Pioneer 11, *J. Geophys. Res., 83*, 717, 1978.

Smith, E. J., M. Neugebauer, A. Balogh, S. J. Bame, R. P. Lepping, and B. T. Tsurutani, Ulysses observations of latitude gradients in the heliospheric magnetic field, *Adv. Space Res., 16*, 165, 1995.

Tang, F., B. T. Tsurutani, W. D. Gonzalez, S. I. Akasofu, and E. J. Smith, Solar sources of interplanetary southward B_z events responsible for major magnetic storms (1978-1979), *J. Geophys. Res., 94*, 3535, 1989.

Timothy, A. F., A. S. Krieger, and G. S. Vaiana, The structure and evolution of coronal holes, *Sol. Phys., 42*, 135, 1975.

Tsurutani, B. T., and W. D. Gonzalez, The cause of high intensity long-duration continuous *AE* activity (HILDCAAs): Interplanetary Alfvén wave trains, *Planet. Space Sci., 35*, 405, 1987.

Tsurutani, B. T. and W. D. Gonzalez The future of geomagnetic storm predictions: Implications from recent solar and interplanetary observations, to appear in *J. Atmos. Terr. Phys.*, 1995a.

Tsurutani, B. T., and W. D. Gonzalez, The efficiency of "viscous

interaction" between the solar wind and the magnetosphere during intense northward IMF events, *Geophys. Res. Lett.*, 22, 663, 1995b.

Tsurutani, B. T., E. J. Smith, K. R. Pyle, and J. A. Simpson, Energetic protons accelerated at corotating shocks: Pioneer 10 and 11 observations from 1 to 6 AU, *J. Geophys. Res.*, 87, 7389, 1982.

Tsurutani, B. T., W. D. Gonzalez, F. Tang, S. I. Akasofu, and E. J. Smith, Origin of interplanetary southward magnetic fields responsible for major magnetic storms near solar maximum (1978-1979), *J. Geophys. Res.*, 93, 8519, 1988.

Tsurutani, B. T., T. Gould, B. E. Goldstein, W. D. Gonzalez, and M. Sugiura, Interplanetary Alfvén waves and auroral (substorm) activity: IMP 8, *J. Geophys. Res.*, 95, 2241, 1990.

Tsurutani, B. T., W. D. Gonzalez, F. Tang, and Y. T. Lee, Great magnetic storms, *Geophys. Res. Lett.*, 19, 73, 1992.

Tsurutani, B. T., C. M. Ho, E. J. Smith, M. Neugebauer, B. E. Goldstein, J. S. Mok, J. K. Arballo, A. Balogh, D. J. Southwood, and W. C. Feldman, The relationship between interplanetary discontinuities and Alfvénic waves: Ulysses observations, *Geophys. Res. Lett.*, 21, 2267, 1994.

Wilcox, J. M., and N. F. Ness, Quasi-stationary corotating structure in the interplanetary medium, *J. Geophys. Res.*, 70, 5793, 1965.

Winterhalter, D., E. J. Smith, M. E. Burton, N. Murphy, and D. J. McComas, The heliospheric plasma sheet, *J. Geophys. Res.*, 99, 6667, 1994.

Zwickl, R. D., J. R. Asbridge, S. J. Bame, W. C. Feldman, J. T. Gosling, and E. J. Smith, Plasma properties of driver gas following interplanetary shocks observed by ISEE-3, in Solar Wind Five, *NASA Conf. Publ.*, CP-2280, 711, 1983.

J. K. Arballo and B. T. Tsurutani, Jet Propulsion Laboratory, California Institute of Technology, MS 169-506, 4800 Oak Grove Drive, Pasadena, CA 91109. (e-mail: jarballo@jplsp.jpl.nasa.gov; btsurutani@jplsp.jpl.nasa.gov)

A. L. C. Gonzalez and W. D. Gonzalez, Instituto National Pesquisas Espaciais (INPE), Sao Jose dos Campos, Sao Paulo, Brazil. (e-mail: gonzalez@das.inpe.br)

M. Okada, National Institute of Polar Research, Tokyo, Japan. (e-mail: mokada@hp9000.nipr.ac.jp)

F. Tang, California Institute of Technology, Pasadena, CA 91125. (e-mail: ft@sunday.caltech.edu)

(Received February 25, 1994; revised May 5, 1995;
accepted May 5, 1995.)